

1 **Magnetic field conditions upstream of Ganymede**

2 Marissa F. Vogt¹, Fran Bagenal², and Scott J. Bolton³

3

4 ¹ Center for Space Physics, Boston University, Boston, MA, USA

5 ² Laboratory for Atmospheric and Space Physics, University of Colorado Boulder, Boulder, CO,
6 USA

7 ³ Southwest Research Institute, San Antonio, TX, USA

8

9 Corresponding Author: Marissa Vogt, mvogt@bu.edu

10

11 **Key points**

- 12 • The magnetic field magnitude and direction upstream of Ganymede vary strongly with
13 longitude
- 14 • Temporal variations in the magnetosphere also influence Ganymede’s upstream field
15 conditions
- 16 • Juno’s Ganymede flyby occurred during typical magnetospheric conditions

17

18 **Abstract**

19 Jupiter’s magnetic field is tilted by $\sim 10^\circ$ with respect to the planet’s spin axis, and as a result the
20 Jovian plasma sheet passes over the Galilean satellites at the jovigraphic equator twice per
21 planetary rotation period. The plasma and magnetic field conditions near Ganymede’s
22 magnetosphere therefore change dramatically every ~ 5 hours, creating a unique magnetosphere-
23 magnetosphere interaction, and on longer time scales as evidenced by orbit-to-orbit variations. In

24 this paper we summarize the typical magnetic field conditions and their variability near
25 Ganymede's orbit as observed by the Galileo and Juno spacecraft. We fit Juno data from orbit
26 34, which included the spacecraft's close Ganymede flyby in June 2021, to a current sheet model
27 and show that the magnetospheric conditions during orbit 34 were very close to the historical
28 average. Our results allow us to infer the upstream conditions at the time of the Juno Ganymede
29 flyby.

30

31 **Plain Language Summary**

32 Ganymede is the only moon in the solar system with an intrinsic magnetic field. This field forms
33 a bubble in space around the moon, called a magnetosphere, that is itself contained within
34 Jupiter's magnetosphere. The magnetic field and plasma conditions within Ganymede's
35 magnetosphere can be used to infer information about the satellite's atmosphere, ionosphere, and
36 interior. It is therefore important to understand the interaction between Ganymede's
37 magnetosphere and the Jovian environment in the same way that we study the effects of space
38 weather on the Earth. Here we analyze Galileo magnetic field measurements from Jupiter's
39 magnetosphere in the region near Ganymede's orbit to establish the typical magnetic field
40 magnitude and direction. We discuss the average conditions as well as the nature of the
41 variability that occurs due to dynamic processes occurring in Jupiter's magnetosphere. This
42 information provides useful context for analyzing data from Juno's recent flyby of Ganymede,
43 which we show occurred during typical magnetospheric conditions.

44

45 **1. Introduction**

46 Jupiter's moon Ganymede is the only satellite in the solar system to possess its own
47 intrinsic magnetic field, which creates a small magnetosphere that is embedded in Jupiter's inner
48 magnetosphere (Kivelson et al., 1996). Ganymede is therefore a fascinating target for studying
49 moon-magnetosphere interactions. Data and models from the Galileo flybys of Io, Europa,
50 Ganymede, and Callisto show that changes in the upstream conditions, including the satellite's
51 location with respect to Jupiter's plasma sheet, can have a major influence on the moon-
52 magnetosphere interaction and produce an inductive response that can be used to probe the
53 moons' internal structure (e.g. Kivelson et al., 1999, 2002). The observed magnetic field from
54 within Ganymede's magnetosphere contains contributions from Ganymede's internal magnetic
55 field, currents within Ganymede's magnetosphere, any inductive magnetic field from a possible
56 subsurface liquid ocean inside the moon, and the magnetic field of Jupiter's magnetosphere
57 (Kivelson et al., 2002). Therefore, it is important to quantify the range of magnetic field and
58 plasma conditions that may be expected upstream of the Galilean satellites and to predict those
59 conditions at the time of close spacecraft encounters.

60 The goals of this paper are 1) to establish the range of likely magnetic field conditions
61 upstream of Ganymede by analyzing the available Galileo and Juno magnetometer data, and 2)
62 to examine the magnetic field conditions near Ganymede during Juno's orbit 34 prior to and
63 following its close flyby of Ganymede on 7 June 2021. We first consider how the magnetic field
64 magnitude and direction near Ganymede change over the ~ 10 hour planetary rotation period as
65 the satellite's magnetic latitude oscillates due to Jupiter's $\sim 10^\circ$ dipole tilt. We then consider how
66 the magnetic field conditions change on longer timescales such as the orbit-by-orbit current sheet
67 variability that has been studied in both Galileo and Juno data (e.g. Russell et al., 2001; Vogt et

68 al., 2017; Connerney et al., 2020). Both of these types of variability in the upstream conditions
69 occur on timescales that are long compared to the ~minutes long timescale for plasma circulation
70 in Ganymede’s magnetosphere (e.g. Jia et al., 2009, 2010; Toth et al., 2016; Zhou et al., 2020)
71 and it is likely that conditions are always favorable for magnetopause reconnection (Kaweeyanun
72 et al., 2020). But even if the upstream field conditions have only a limited influence on activity
73 in Ganymede’s magnetosphere, they can still affect the interpretation of magnetic field
74 measurements near Ganymede. In particular, the magnetic field observed near Ganymede
75 includes the contributions of both Jupiter’s magnetosphere field and the field produced by
76 Ganymede (intrinsic and induced), so an accurate estimate of the upstream conditions is
77 important to constraining the properties of Ganymede’s internal magnetic field. In our study we
78 focus on the upstream magnetic field conditions though the plasma conditions are also both
79 temporally and spatially variable (e.g. Kivelson et al., 2022), which will affect the nature of the
80 satellite-magnetosphere interaction (e.g. Bagenal and Dols, 2020).

81 This paper is organized as follows: section 2 reviews the availability of magnetic field
82 measurements near Ganymede’s orbit and the expected dependence on longitude. Section 3
83 summarizes the Galileo magnetic field measurements near Ganymede and their spatial
84 (longitudinal and local time) and temporal variability. In section 4 we examine the
85 magnetospheric conditions before and after Juno’s orbit 34 Ganymede flyby, and we conclude
86 with a summary in section 5.

87

88 **2. Data availability and expected longitudinal dependence**

89 Magnetic field measurements from Jupiter’s magnetosphere are available from six
90 spacecraft that flew through the system (Voyager 1, Voyager 2, Pioneer 10, Pioneer 11, Ulysses)

91 and two orbiters (Galileo, 1996-2003; and Juno, 2016-present). Figure 1 shows the orbital
92 coverage of all spacecraft that have visited the Jovian system except Cassini, which only briefly
93 entered Jupiter’s magnetosphere, and New Horizons, which did not carry a magnetometer. The
94 spacecraft trajectories are shown in magnetospheric local time, System III latitude and longitude,
95 and magnetic coordinates (“wobble plot”) as calculated using the JRM09 dipole tilt value of
96 10.31° toward 196.61° System III left-handed longitude (Connerney et al., 2018). Galileo’s orbit
97 was confined to near the jovigraphic equatorial plane while Juno is in a polar 53-day orbit with
98 an apoapsis of $\sim 110 R_J$ and an inclination that is increasing with time (Bolton et al., 2017).
99 During the inbound portion of its initial orbits Juno’s latitude at ~ 10 - $20 R_J$ was as large as $\sim 20^\circ$
100 but that latitude has decreased with time.

101 Ganymede orbits Jupiter in a nearly circular path (eccentricity = 0.001) with a semi-major
102 axis $14.97 R_J$ ($1 R_J = 71,492$ km) and an orbital inclination of 0.18° . For simplicity, in our
103 analysis we will take “Ganymede’s orbit” to mean a circular path of radius $15 R_J$ in Jupiter’s
104 jovigraphic equatorial plane. Most of the magnetic field measurements from the region near
105 Ganymede’s orbit come from Galileo, which completed over 30 orbits of Jupiter and collected
106 magnetic field measurements with a typical time resolution of 24 seconds per vector. In just
107 under half of its first 34 orbits, Juno passed through magnetic latitudes equivalent to the region
108 near Ganymede’s orbit, as shown in the bottom middle panel of Figure 1, though the spacecraft
109 was typically located $\sim 1 R_J$ or more off the jovigraphic equator (see top right panel of Figure 1).
110 Juno magnetic field measurements are available with a time resolution of 1 second per vector
111 (Connerney et al., 2017). The other spacecraft that passed Ganymede’s orbit (Pioneer 10, Pioneer
112 11, Voyager 1, Voyager 2, Ulysses) were typically located significantly off the jovigraphic
113 equator, so we exclude them from our statistical analysis in the next section.

114 The magnetic field in Jupiter’s innermost magnetosphere ($R < 10 R_J$) is largely dipolar,
115 while in the middle magnetosphere ($R > 30 R_J$) the field becomes radially stretched by the
116 currents flowing in the current sheet or plasma sheet. Outside of the Io plasma torus, the plasma
117 in Jupiter’s magnetosphere is concentrated in a plasma sheet that is roughly aligned with the
118 magnetic equator inside of $\sim 30 R_J$ (Behannon et al., 1981). At Ganymede’s orbit the magnetic
119 equator and centrifugal equator, the point along each flux tube farthest from the planet, are
120 nearly, but not exactly, aligned (Phipps and Bagenal, 2021). Jupiter’s dipole field is tilted $\sim 10^\circ$
121 with respect to the planet’s spin axis, toward $\sim 200^\circ$ west (left-handed) System III longitude. As a
122 result, a spacecraft or moon near the jovigraphic equator – like Galileo and Ganymede – will
123 observe the magnetic field fluctuating as its magnetic latitude oscillates from roughly $+10^\circ$ to -
124 10° over the planet’s ~ 10 hour rotation period. Therefore, both the magnitude and direction of the
125 magnetic field upstream of Ganymede are strongly dependent on longitude. For example, the
126 radial component of the magnetic field, B_R , reverses twice per planetary rotation as Jupiter’s
127 plasma sheet passes over the jovigraphic equator.

128 Figure 2, which we discuss further in the next section, shows the modeled longitudinal
129 dependence of the magnetic field at Ganymede’s orbit along with Galileo measurements from
130 radial distances 14.95-15.05 R_J . A similar plot showing the longitudinal dependence of the
131 magnetic field near Ganymede’s orbit as measured during Juno’s first 33 orbits is given in Figure
132 3; we exclude Juno data from Figure 2 because most orbits are significantly off the jovigraphic
133 equator and therefore are not representative of the magnetic field conditions near Ganymede. The
134 model field, shown by the thick gray lines, is calculated using the JRM09 model for Jupiter’s
135 internal field plus the contribution of a current sheet from the Connerney et al. (2020) model
136 (“CON2020”) at a radial distance of 15 R_J at the jovigraphic equator. This current sheet model is

137 based on a Voyager-era model which represented Jupiter’s current sheet as an axisymmetric
 138 washer-shaped disk (Connerney et al., 1981). The Voyager-era model fit parameters are the inner
 139 and outer edge of the disk, the disk thickness, the current sheet azimuthal tilt, the azimuthal angle
 140 of the tilt, and the azimuthal current constant $\frac{\mu_0 I_0}{2}$, which represents the current sheet current
 141 density and is given in units of nT. The CON2020 model updated the original Voyager-era
 142 model by introducing a radial current constant I_{rad} , in units of MA, that produces a B_ϕ , the
 143 azimuthal component of the magnetic field, and controls the field bend back out of the meridian
 144 plane. Fitting the current constants to Galileo and Juno data on an orbit-by-orbit basis has
 145 provided a measurement of temporal activity in Jupiter’s magnetosphere and can give insights
 146 into the expected field variability at Ganymede’s orbit (Vogt et al., 2017; Connerney et al.,
 147 2020). Finally, we note that other external field models (e.g. Khurana, 1997) predict similar
 148 magnetic field conditions near Ganymede’s orbit, as shown in Figure S1.

149

150 **3. Galileo magnetic field observations near Ganymede: spatial and temporal variability**

151 The measurements and model predictions plotted in Figure 2 provide an overview of the
 152 typical magnetic field conditions upstream of Ganymede and their spatial and temporal
 153 variability. The figure shows the three field components in System III spherical coordinates, the
 154 magnetic field bendback and elevation angles, and the field magnitude as a function of longitude.
 155 The magnetic field bendback angle α indicates the angle of the magnetic field out of a meridian
 156 plane and is defined by $\alpha = \tan^{-1} \left(\frac{B_\phi}{B_R} \right)$ so that a negative (positive) bendback angle indicates a
 157 swept back (swept forward) field configuration. The field elevation angle, $\theta_{elevation}$, indicates the
 158 angle that the magnetic field makes with respect to the radial direction in the R - θ plane and is

159 defined by $\theta_{elevation} = \tan^{-1}\left(\frac{-B_\theta}{|B_R|}\right)$ so that the elevation angle is positive for a southward field
160 and is 90° when the field is completely southward. We evaluate both angles only when $|B_R| > 3$
161 nT because small fluctuations in B_R can lead to large fluctuations in the field angles when B_R is
162 small. The data plotted in Figure 2 are clustered in groups that each come from individual orbit
163 inbound or outbound segments, with color indicating the spacecraft local time. Figure 2 includes
164 all Galileo measurements at radial distances 14.95-15.05 R_J excepting the six close flybys of
165 Ganymede when the spacecraft was measuring Ganymede's magnetospheric field. For the
166 intervals plotted in Figure 2, the Galileo spacecraft was located at jovigraphic latitudes -1.57° to
167 3.27° .

168 The data and model predictions in Figure 2 show overall good agreement and can be used
169 together to characterize the magnetic field conditions near Ganymede's orbit, which we
170 summarize in Table 1. The measurements listed in Table 1 describe the range of field values
171 measured by Galileo, excluding the close flyby encounters, at radial distances 14.95-15.05 R_J .
172 The average $|B|$ value near Ganymede is ~ 95 -100 nT according to both the data and model, and
173 the field is typically oriented mostly in the north-south direction and only weakly swept out of
174 the meridian plane (the model predicts $|B_\theta| > |B_R|$ and $|\alpha| < 20^\circ$ at roughly 70 percent of
175 longitudes). The magnetic field orientation is therefore generally favorable for reconnection at
176 Ganymede's magnetopause since the satellite's internal magnetic field is oriented almost
177 completely northward, with a dipole tilt of 176° from its spin axis (Kivelson et al., 2002;
178 Kaweeyanun et al., 2020).

179 The field near Ganymede's orbit changes on time scales that are longer than the ~ 10 hour
180 planetary rotation period, as shown by orbit-to-orbit changes in the observed field values plotted
181 in Figure 2. Some of the orbit-to-orbit variation may be accounted for by the orbits' spatial, not

182 temporal, differences. For example, the magnetic field and plasma properties in Jupiter's
183 magnetosphere vary with local time (e.g. Palmaerts et al., 2017 and references therein), which
184 means that the upstream magnetic field conditions change over the satellite's ~ 7 day orbital
185 period. The local time dependence of the magnetic field is most evident in the meridional
186 component, B_θ , which varies by ~ 9 nT ($\sim 10\%$) near Ganymede's orbit. Galileo measurements of
187 the B_θ local time dependence near Ganymede are plotted in Figure S2, which shows that the data
188 are reasonably well-fit by the longitudinally-averaged JRM09+CON2020 model plus the external
189 B_θ local time fit of Vogt et al. (2017). The B_θ local time dependence can also be seen in Figure
190 2, as B_θ measurements collected at local times near 15:00 (purple and dark blue) are generally
191 larger than those collected at local times far from 15:00 (green and red). We account for local
192 time variations in the functional fits described in Appendix A. However, most of the orbit-to-
193 orbit variability in the magnetic field indicates variable magnetospheric conditions due to activity
194 like magnetospheric injections, mass loading due to volcanic activity on Io, or even changes in
195 the external solar wind conditions (e.g. Mauk et al., 1999; Louarn et al., 2014; Tao et al., 2005;
196 Vogt et al., 2019).

197 In general, the magnitude of these orbit-by-orbit temporal changes is significantly smaller
198 than the magnitude of the variations with longitude. For example, the two dashed gray lines in
199 Figure 2 show the expected range of the JRM09 + CON2020 modeled field conditions. To
200 calculate these maximum and minimum model values we used the range of best fit current
201 constants fit to individual Juno orbits listed in Table 2 of Connerney et al. (2020). The average
202 temporal change in $|B|$ expected from the current sheet variability is ~ 5 nT, but it can be as large
203 as ~ 12 nT near the magnetic equator. The modeled differences in the individual field
204 components, which we list in Table 1, typically represent a ~ 10 -20 percent variability in the

205 baseline values (note that the change in B_R and B_ϕ depends strongly on longitude). Figure S3
206 illustrates how changes in the CON2020 current constants affect the predicted individual field
207 components near Ganymede’s orbit. In general, changes to the radial current constant I_{rad} have
208 only a very small effect on B_R and B_θ but can significantly influence B_ϕ , particularly at high
209 magnetic latitudes (near the longitude of the dipole tilt and 180° away from it). Near the
210 magnetic equator only B_θ is strongly dependent on the azimuthal current constant $\frac{\mu_0 I_0}{2}$.

211 Connerney et al. (2020) reported that the current sheet variability during Juno’s first 24
212 orbits, as determined by orbit-to-orbit changes in best-fit current constants, was roughly
213 comparable to the variability reported in Galileo data by Vogt et al. (2017). However, the Juno
214 measurements plotted in Figure 3 show significantly greater orbit-to-orbit variability than do the
215 Galileo data from Figure 2. It is therefore important to note that the Juno data were collected at a
216 larger range of jovigraphic latitudes than the near-equatorial Galileo data. Data in Figure 3 are
217 plotted in colors indicating the average jovigraphic latitude of the spacecraft during the interval
218 plotted for each orbit. The thin colored lines in Figure 3 show the longitudinal dependence of the
219 JRM09+CON2020 model field at different jovigraphic latitudes. At the highest latitudes shown
220 (15° and 20° latitude, in light and dark blue, respectively) the model field differs significantly
221 from the near-equatorial field (e.g. 0° and 5° latitude, plotted in red and yellow, respectively) in
222 terms of its magnitude, direction, and longitudinal dependence. Therefore, it is important to
223 consider the latitude at which the Juno data were measured and compare Juno data only to model
224 predictions evaluated at similar latitudes (e.g. by comparing data to a model line of a similar
225 color in Figure 3). Though the Juno magnetic field data in Figure 3 display greater overall
226 variability than the near-equatorial Galileo data in Figure 2 we conclude that most of that
227 variability is due to the large latitudinal range of Juno’s orbits.

228 In Figure 4 we show the values of the magnetic field measured by Galileo in the general
229 vicinity of Ganymede, organized by position in magnetic cylindrical coordinates. Each panel is
230 divided into boxes spanning $0.05 R_J$ in ρ_{mag} (cylindrical radial distance) by $0.25 R_J$ in z_{mag} , with
231 color indicating quantities like the average or standard deviation of the measured magnetic field
232 in each box. This figure gives insight into the expected field variability at Ganymede’s orbit on
233 both short (~ 10 hour) and long (orbit-by-orbit) time scales. The average B_R is very well-
234 organized by magnetic coordinates, indicating that the B_R near Ganymede is relatively constant
235 on long time scales (weeks to months) but varies strongly as Ganymede’s position in magnetic
236 coordinates (pink curves in Figure 4) change over a planetary rotation period. By comparison,
237 the plot of the average B_ϕ is extremely disorganized, indicating that it is highly variable on long
238 time scales.

239 Figure 4 also shows that the long-term temporal variability of B_R and B_θ , as indicated by
240 the standard deviation plots, is typically \sim a few nT, which is roughly consistent with the
241 CON2020 modeled temporal variability. This can also be seen in Figure 2, where the magnitude
242 of the scatter in B_R and B_θ at a given longitude is roughly consistent with the modeled current
243 sheet variability (the difference between the two dashed gray lines) but the scatter in the
244 measured B_ϕ is significantly larger than the temporal variability predicted by the CON2020
245 model. Analogous plots made using Juno data are provided in Figure S4, though we note that
246 each colored box typically contains data from only one Juno orbit because of the limited data
247 coverage at low jovigraphic latitudes. Therefore, the standard deviations plotted in Figure S4, are
248 typically smaller for Juno than for Galileo because they indicate temporal variability on short
249 (seconds or minutes) timescales rather than orbit-to-orbit variability.

250 Finally, in Appendix A we derive functional fits to the Galileo magnetic field
251 measurements near Ganymede. Existing global field models, including the JRM09 + CON2020
252 model and the Khurana (1997) model, show good agreement with the data throughout the inner
253 and middle magnetosphere. However, by focusing just on the data collected near Ganymede and
254 by including variability with local time, our functional fits quantitatively improve on the data-
255 model agreement and provide a simple functional form for the magnetic field conditions near
256 Ganymede.

257

258 **4. Magnetospheric conditions at the time of Juno’s Ganymede flyby**

259 Juno’s close Ganymede flyby occurred on 7 June 2021, with closest approach at 16:56
260 UT at a subspacecraft SIII right handed longitude of 57.5° (Hansen et al., this issue). The
261 spacecraft encountered Ganymede’s magnetosphere and wake at SIII right handed longitudes
262 $\sim 70^\circ$ to $\sim 50^\circ$, when Ganymede was just south of the magnetic equator and very close to the
263 center of the plasma sheet. (A radial distance of $15 R_J$ at the jovigraphic equator and SIII
264 longitudes 50° to 70° corresponds to magnetic latitudes of -4.1° to 0.7° and z_{mag} from $-1.07 R_J$ to $-$
265 $0.16 R_J$.) We follow three steps in estimating the magnetic field conditions upstream of
266 Ganymede.

267 First, we consider the predicted conditions using the JRM09 + CON2020 average and
268 temporally varying model. The JRM09 + CON2020 model (with average current constant
269 values) predicts the following field values for SIII longitudes 50° - 70° (see Table 2): $B_R \sim -29$ nT
270 to ~ 0 nT, $B_\theta \sim 69$ nT, $B_\phi \sim -10$ nT to -13 nT, $|B| \sim 76$ nT to 71 nT, bendback angle $\sim 20^\circ$ - 85° ,
271 and elevation angle $\sim 70^\circ$ - 89° . At those longitudes, using the largest or smallest best fit values of
272 the CON2020 current constants rather than the average values would change the modeled field

273 components roughly as follows: $B_R \pm 1$ nT, $B_\theta \pm 6$ nT, $B_\phi \pm 1$ nT, $|B| \pm 5$ nT. This gives us the
274 full range of expected field conditions at the time of Juno’s Ganymede flyby and shows that the
275 individual field components and field magnitude can vary by as much as ± 5 -10 percent of their
276 average values.

277 Second, we fit the data to the CON2020 model to obtain a rough estimate of the best fit
278 current constants to evaluate the state of the magnetosphere during orbit 34. We followed Vogt et
279 al. (2017) in varying only the $\frac{\mu_0 I_0}{2}$ parameter to fit B_θ , at radial distances 10 to 30 R_J during each
280 orbit’s inbound pass and excluding the Ganymede flyby interval during orbit 34. We then fit the
281 measured B_ϕ by varying the radial current constant value with the best fit $\mu_0 I_0$ calculated for
282 each orbit. For both $\frac{\mu_0 I_0}{2}$ and I_{rad} we estimated the best fit by calculating the model field at a
283 range of values (with a 2 nT step size) and minimizing the root mean square error between the
284 external (measured – JRM09 internal field) and model field. Though our approach differs
285 slightly from Connerney et al. (2020) we obtained nearly identical best fit $\mu_0 I_0$ values for Juno’s
286 first 24 orbits (see Figure S5), which gives us confidence in the validity of our fits estimates. We
287 found that the first 34 Juno orbits featured an average $\frac{\mu_0 I_0}{2}$ fit of 144.3 nT (standard deviation 8.5
288 nT), consistent with the average 140.2 nT Connerney et al. (2020) reported from Juno’s first 24
289 orbits. For orbit 34 we calculated a best fit $\frac{\mu_0 I_0}{2}$ fit of 138 nT, slightly below average. Our
290 calculated best fit I_{rad} was 44 MA, though we note that the goodness of the B_ϕ fit was nearly
291 independent of the radial current constant in orbit 34 and that our fit approach closely reproduced
292 the Connerney et al. (2020) $\frac{\mu_0 I_0}{2}$ fit value but not the I_{rad} (our average was 23.8 MA, compared
293 to 16.7 MA from Connerney et al. (2020); see Figure S6).

294 Finally, we compare the field measured by Juno during orbit 34 to the Galileo average
295 along Juno’s trajectory in magnetic coordinates, as shown in Figure 5. The black lines show Juno
296 orbit 34 data as a function of ρ_{mag} , while the red lines in each panel show the Galileo average
297 magnetic field values in each (ρ_{mag}, z_{mag}) bin from Figure 4 along Juno’s trajectory (thick white
298 line in Figure 4), and error bars show the standard deviation within the bins. This comparison
299 shows that the magnetic field conditions in Jupiter’s magnetosphere immediately before and after
300 Juno’s close Ganymede flyby were, overall, within the range of the typical Galileo
301 measurements. The Juno field magnitude is typically slightly smaller than the Galileo averages,
302 due in part to differences in B_ϕ , which is highly variable in this area. However, the Juno B_θ
303 values are also systematically slightly smaller than the Galileo averages, which is consistent with
304 Connerney et al. (2020)’s finding that the Juno-era height-integrated current in the magnetodisk
305 is $\sim 15\%$ smaller than in the Pioneer, Voyager, and Galileo eras.

306 Overall, we find that the magnetic field measurements near Ganymede’s orbit from Juno
307 orbit 34 are well-described by the JRM09 internal field plus the *average* CON2020 model
308 external field (blue lines in Figure 5). Only the B_ϕ component is systematically poorly fit by both
309 the average Galileo field and by the JRM09+CON2020 model; the model field predicts $B_\phi \sim -11$
310 nT at Ganymede though the observed B_ϕ is ~ -14 nT. The average model would therefore
311 provide a good estimate of Jupiter’s magnetospheric field during the flyby, though a better fit
312 would use the slightly modified current constant parameters and would manually adjust the B_ϕ
313 fit. Overall, the measured $|B|$ near Ganymede’s orbit during Juno orbit 34 differs from the
314 average JRM09+CON2020 model $|B|$ by only about ~ 2 percent and there is no systematic offset
315 in $|B|$ or in B_θ as one would expect if the magnetodisk currents were significantly different from
316 their average values.

317

318 **5. Conclusions and Summary**

319 The magnetic field conditions upstream of Ganymede display both spatial and temporal
320 variability that can influence the moon-magnetosphere interaction. The spatial variability
321 includes a local time dependence and, most significantly, a dependence on longitude due to
322 Jupiter's $\sim 10^\circ$ dipole tilt. The longitudinal dependence is significantly larger than the observed
323 orbit-to-orbit variability, with $|B|$ fluctuating from ~ 65 to ~ 125 nT during each planetary rotation.
324 The field direction also varies significantly, with the bendback angle ranging from roughly -85°
325 (almost completely swept back) to $+85^\circ$ (almost completely swept forward) and the elevation
326 angle ranging from $\sim 35^\circ$ to $\sim 90^\circ$ (completely southward).

327 Galileo data from near the jovigraphic equator show that the longitudinal dependence of
328 the magnetic field near Ganymede's orbit is well-described by the combined JRM09 internal
329 field model (Connerney et al., 2018) and CON2020 external field model (Connerney et al.,
330 2020), which computes the field due to Jupiter's current sheet. The CON2020 model includes
331 azimuthal and radial current constant parameters that can be fit to data from each Galileo or Juno
332 orbit to obtain a measure of the variability in Jupiter's magnetodisk. The expected orbit-to-orbit
333 temporal variability obtained from these current sheet fits represents a ~ 10 - 20 percent variability
334 in the baseline values of the individual field components and $|B|$, though the exact details depend
335 on longitude. This possible variability should be considered when making preparations, such as
336 reanalysis of Galileo flyby data or modeling work, for the upcoming NASA Europa Clipper and
337 ESA JUICE missions.

338 During orbit 34, Juno flew past Ganymede at SIII right handed longitudes $\sim 70^\circ$ to $\sim 50^\circ$,
339 when Ganymede was just south of the magnetic equator and very close to the center of the

340 plasma sheet. At these longitudes the expected average field conditions based on the
341 JRM09+CON2020 model would be: $B_R \sim -29$ nT to ~ 0 nT, $B_\theta \sim 69$ nT, $B_\phi \sim -10$ nT to -13 nT,
342 $|B| \sim 76$ nT to 71 nT, bendback angle $\sim 20^\circ$ - 85° , and elevation angle $\sim 70^\circ$ - 89° . We calculated the
343 best fit current constant parameters to Juno magnetic field data from orbit 34 and also compared
344 the magnetic field along Juno's trajectory to Galileo averages from the same positions in
345 magnetic coordinates. Our analysis showed that Jupiter's magnetospheric field during orbit 34
346 was very close to its average state. Overall, the orbit 34 data near Ganymede's orbit are well-
347 described by the JRM09+CON2020 average model, with only the B_ϕ component being
348 systematically underestimated in magnitude (predicted -11 nT compared to -14 nT observed).
349 We look forward to future Juno, Europa Clipper, and JUICE data from Jupiter's inner
350 magnetosphere that should provide new insight into the nature and causes of the temporal
351 variability in Jupiter's magnetodisk and its influence on the plasma environments of the Galilean
352 satellites.

353

354 **Appendix A: Functional fits to magnetic field data near Ganymede**

355 We have derived simple functional fits to the Galileo magnetic field measurements near
356 Ganymede, including all data from radial distances 14.95 - $15.05 R_J$ (i.e. the data presented in
357 Figure 2) except orbit C9, which occurred near 50° longitude, when B_θ and $|B|$ were anomalously
358 small due to a likely current sheet crossing. At Ganymede's orbit the internal magnetic field is
359 very well-approximated by a dipole field; at a radial distance of $15 R_J$ in the jovigraphic equator
360 the longitudinally-average difference between the full JRM09 field model and the JRM09 dipole
361 field (same tilt and dipole moment) is just ~ 1.5 percent of the field magnitude. We therefore
362 chose to represent the field near Ganymede as the sum of a tilted dipole – using the values for the

363 dipole moment and tilt from the JRM09 model – and an external field that does not depend on
 364 magnetic longitude but does vary with local time.

365 Based on qualitative and rough quantitative assessments of how the Galileo data and the
 366 CON2020 external field vary spatially, we chose the following functional forms for the magnetic
 367 field in cylindrical magnetic coordinates:

$$368 \quad B_{\rho,ext} = \frac{z}{\sqrt{\rho}} (A + B \cos(\psi - C)) \quad (A1)$$

$$369 \quad B_{\phi,ext} = \frac{z}{\rho} (D + E \cos(\psi - F)) \quad (A2)$$

$$370 \quad B_{z,ext} = \frac{1}{\rho} (G + H \cos(\psi - I)) \quad (A3)$$

371 where $A, B, C, D, E, F, G, H,$ and I are constants to be obtained by fitting, ρ and z are cylindrical
 372 magnetic coordinates in Jovian radii (R_J), ψ is local time in radians, and all field components are
 373 in units of nT. We note that parameters $B, E,$ and H indicate the magnitude of the local time
 374 dependence of $B_{\rho,ext}, B_{\phi,ext},$ and $B_{z,ext},$ respectively, while $C, F,$ and I indicate the phase of the
 375 local time dependence.

376 We first estimated the measured external field by subtracting the JRM09 dipole field
 377 from the observed magnetic field values. We then fit the measured external field components to
 378 eqs. 1-3 using the IDL function `curvefit`, obtaining the following values for the fit parameters: A
 379 $= 49.87, B = 6.41, C = 4.74$ hours, $D = -6.87, E = -8.93, F = 6.88$ hours, $G = 707.98$ nT, $H = -$
 380 133.38 nT, $I = 14.80$ hours. The magnitude of the local time dependence is ~ 10 - 20 percent of the
 381 background value for $B_{\rho,ext}, B_{z,ext}$ but substantially larger for $B_{\phi,ext},$ probably because of the
 382 relatively large amount of scatter in B_{ϕ} (see Figure 4). The magnitude of $B_{\rho,ext}$ and $B_{\phi,ext}$ both
 383 peak near dawn, consistent with observations showing a more radially stretched field and thin
 384 current sheet near dawn than near dusk (e.g. Palmaerts et al., 2017). The minimum in $B_{z,ext},$

385 which corresponds to the peak in B_θ , occurs near 15:00 LT, which is consistent with the 2-D fit
 386 of Vogt et al. (2011).

387 Table A1 compares the RMS error between the Galileo measurements and the functional
 388 fits we have derived here to the RMS error obtained using JRM09 with either CON2020 or the
 389 Khurana (1997) external field. Though this functional fit is only applicable very close to
 390 Ganymede's orbit (15 R_J at the jovigraphic equator), it does a substantially better job of
 391 matching the B_θ field component, and reduces the RMS error for B_ϕ and $|B|$, compared to both
 392 field models. The 7.76 nT RMS error in $|B|$ represents a ~ 7.7 percent error in the average
 393 measured $|B|$.

394 Figure A1 shows our functional fits, rotated into SIII coordinates, as a function of
 395 longitude. The field was evaluated at 15 R_J in the jovigraphic equator as a function of longitude
 396 at noon (blue) and midnight (red) local times and is plotted along with the average CON2020
 397 field (black solid lines) and Khurana (1997) model field (black dashed lines). The magnitude and
 398 longitudinal profile of our functional fit and CON2020 are very similar.

399 For both Galileo and Juno, the measured magnetic field and its spatial dependence is
 400 commonly expressed in SIII coordinates, though we calculated our functional fit in magnetic
 401 cylindrical coordinates. Therefore, we briefly describe here the equations needed to rotate from
 402 magnetic to SIII coordinates. The rotation from SIII spherical coordinates (r, θ, φ) to cartesian
 403 magnetic coordinates $(x_{mag}, y_{mag}, z_{mag})$ where z_{mag} is aligned with the dipole axis, which is tilted
 404 by an angle θ_d toward jovigraphic longitude φ_d , and x_{mag} points toward jovigraphic longitude
 405 φ_d , is given by:

$$406 \quad x_{mag} = r[\sin \theta \cos(\varphi - \varphi_d) \cos \theta_d - \cos \theta \sin \theta_d] \quad (A4)$$

$$407 \quad y_{mag} = r \sin \theta \sin(\varphi - \varphi_d) \quad (A5)$$

408
$$z_{mag} = r[\cos \theta \cos \theta_d + \sin \theta \cos(\varphi - \varphi_d) \sin \theta_d] \quad (A6)$$

409 For the JRM09 dipole, $\theta_d = 10.31^\circ$ and $\varphi_d = 163.39^\circ$ in right-handed longitude.

410 The full magnetic field of the functional fit is calculated by adding the dipole and
411 external field components in magnetic cylindrical coordinates:

412
$$B_\rho = B_{\rho,dipole} + B_{\rho,ext} \quad (A7)$$

413
$$B_\phi = B_{\phi,dipole} + B_{\phi,ext} \quad (A8)$$

414
$$B_z = B_{z,dipole} + B_{z,ext} \quad (A9)$$

415 The dipole field can be calculated from the usual equations using the JRM09 dipole moment $M =$
416 4.170 G (Connerney et al., 2018). The simplest way to rotate the field from magnetic cylindrical
417 coordinates to SIII cartesian coordinates is to first convert from magnetic cylindrical coordinates
418 to magnetic cartesian coordinates $(B_{x,mag}, B_{y,mag}, B_{z,mag})$ then rotate into SIII cartesian coordinates
419 following:

420
$$B_{x,SIII} = (B_{x,mag} \cos \theta_d + B_{z,mag} \sin \theta_d) \cos \varphi_d - B_{y,mag} \sin \varphi_d \quad (A10)$$

421
$$B_{y,SIII} = B_{y,mag} \cos \varphi_d + (B_{x,mag} \cos \theta_d + B_{z,mag} \sin \theta_d) \sin \varphi_d \quad (A11)$$

422
$$B_{z,SIII} = B_{z,mag} \cos \theta_d - B_{x,mag} \sin \theta_d . \quad (A12)$$

423 Finally, the field can then be converted from SIII cartesian to SIII spherical coordinates using the
424 typical equations.

425

426

427 **Acknowledgements**

428 We gratefully acknowledge helpful discussions with Jack Connerney and constructive comments
429 from Xianzhe Jia and an anonymous reviewer. The JRM09 + CAN2020 current sheet code used
430 to create several figures was developed by M.F.V. in collaboration with Rob Wilson, Gabby

431 Provan, Matt James, and Marty Brennan and is available at <https://github.com/rjwilson->
432 LASP/PSH and https://github.com/marissav06/con2020_idl. Magnetometer data from all
433 spacecraft that have visited the Jovian system are available from the Planetary Data System.
434 Specifically, Galileo data can be downloaded from <https://pds->
435 [ppi.igpp.ucla.edu/search/?sc=Galileo&t=Jupiter&i=MAG](https://pds-ppi.igpp.ucla.edu/search/?sc=Galileo&t=Jupiter&i=MAG), and Juno data can be downloaded
436 from <https://pds-ppi.igpp.ucla.edu/search/?sc=Juno&t=Jupiter&i=FGM>. M.F.V. was supported
437 by NASA grant 80NSSC20K0559 and by the Juno Participating Scientist program.

438 **References**

439

440 Bagenal, F., & Dols, V. (2020). The space environment of Io and Europa. *Journal of Geophysical*
441 *Research: Space Physics*, 125, e2019JA027485. <https://doi.org/10.1029/2019JA027485>

442

443 Behannon, K. W., L. F. Burlaga, and N. F. Ness (1981), The Jovian magnetotail and its current
444 sheet, *J. Geophys. Res.*, 86, 8385-8401.

445

446 Bolton, S.J., Lunine, J., Stevenson, D. et al. *Space Sci Rev* (2017) 213: 5.
447 <https://doi.org/10.1007/s11214-017-0429-6>

448

449 Connerney, J., M. Acuña, and N. Ness (1981), Modeling the Jovian Current Sheet and Inner
450 Magnetosphere, *J. Geophys. Res.*, 86(A10), 8370-8384.

451

452 Connerney, J.E.P., Benn, M., Bjarno, J.B., Denver, T., Espley, J., Jorgensen, J.L., et al. (2017).
453 The Juno magnetic field investigation, *Space Sci. Rev.*, 213(1-4), 39-138, doi: 10.1007/s11214-
454 017-0334-z.

455

456 Connerney, J. E. P., Kotsiaros, S., Oliverson, R. J., Espley, J. R., Joergensen, J. L., Joergensen, P.
457 S., et al. (2018). A new model of Jupiter's magnetic field from Juno's first nine orbits.
458 *Geophysical Research Letters*, 45. <https://doi.org/10.1002/2018GL077312>

459

460 Connerney, J. E. P., Timmins, S., Hecceg, M., & Joergensen, J. L. (2020). A Jovian magnetodisc
461 model for the Juno era. *Journal of Geophysical Research: Space Physics*, 125, e2020JA028138.
462 <https://doi.org/10.1029/2020JA028138>

463

464 Hansen, C. J, et al., Juno's Close Encounter with Ganymede – an Overview, submitted to
465 *Geophys. Res. Lett.*, this issue.

466

467 Jia, X., Walker, R. J., Kivelson, M. G., Khurana, K. K., and Linker, J. A. (2009), Properties of
468 Ganymede's magnetosphere inferred from improved three-dimensional MHD simulations, *J.*
469 *Geophys. Res.*, 114, A09209, doi:10.1029/2009JA014375.

470

471 Jia, X., Walker, R. J., Kivelson, M. G., Khurana, K. K., and Linker, J. A. (2010), Dynamics of
472 Ganymede's magnetopause: Intermittent reconnection under steady external conditions, *J.*
473 *Geophys. Res.*, 115, A12202, doi:10.1029/2010JA015771.

474

475 Kaweeyanun, N., Masters, A., & Jia, X. (2020). Favorable conditions for magnetic reconnection
476 at Ganymede's upstream magnetopause. *Geophysical Research Letters*, 47, e2019GL086228.

477 <https://doi.org/10.1029/2019GL086228>

478

479 Khurana, K. K. (1997), Euler potential models of Jupiter's magnetospheric field, *J. Geophys.*
480 *Res.*, 102(A6), 11295-11306.

481

482 Kivelson, M. G., K. K. Khurana, C. T. Russell, R. J. Walker, J. Warnecke, F. V. Coroniti, C.
483 Polanskey, D. J. Southwood, and G. Schubert (1996), Discovery of Ganymede's magnetic field
484 by the Galileo spacecraft, *Nature*, 384, 537 - 541.
485

486 Kivelson, M. G., Khurana, K. K., Stevenson, D. J., Bennett, L., Joy, S., Russell, C. T., Walker,
487 R. J., Zimmer, C., and Polanskey, C. (1999), Europa and Callisto: Induced or intrinsic fields in a
488 periodically varying plasma environment, *J. Geophys. Res.*, 104(A3), 4609– 4625,
489 doi:10.1029/1998JA900095.
490

491 Kivelson, M.G., Khurana, K. K., & Volwerk, M. (2002), The permanent and inductive magnetic
492 moments of Ganymede, *Icarus*, 157, 507–522, doi:10.1006/icar.2002.6834.
493

494 Kivelson, M. G. et al., “Ganymede: Its Magnetosphere and its Interaction with the Jovian
495 Magnetosphere”, in: “Ganymede”, eds. M. Volwerk, M. McGrath, X. Jia and T. Spohn,
496 Cambridge University Press, Cambridge, UK, pre-press, 2022.
497

498 Louarn, P., C. P. Paranicas, and W. S. Kurth (2014), Global magnetodisk disturbances and energetic
499 particle injections at Jupiter, *J. Geophys. Res. Space Physics*, 119, 4495–4511,
500 doi:10.1002/2014JA019846.
501

502 Mauk, B. H., D. J. Williams, R. W. McEntire, K. K. Khurana, and J. G. Roederer (1999), Storm-
503 like dynamics of Jupiter's inner magnetosphere, *J. Geophys. Res.*, 104, 22,759.
504

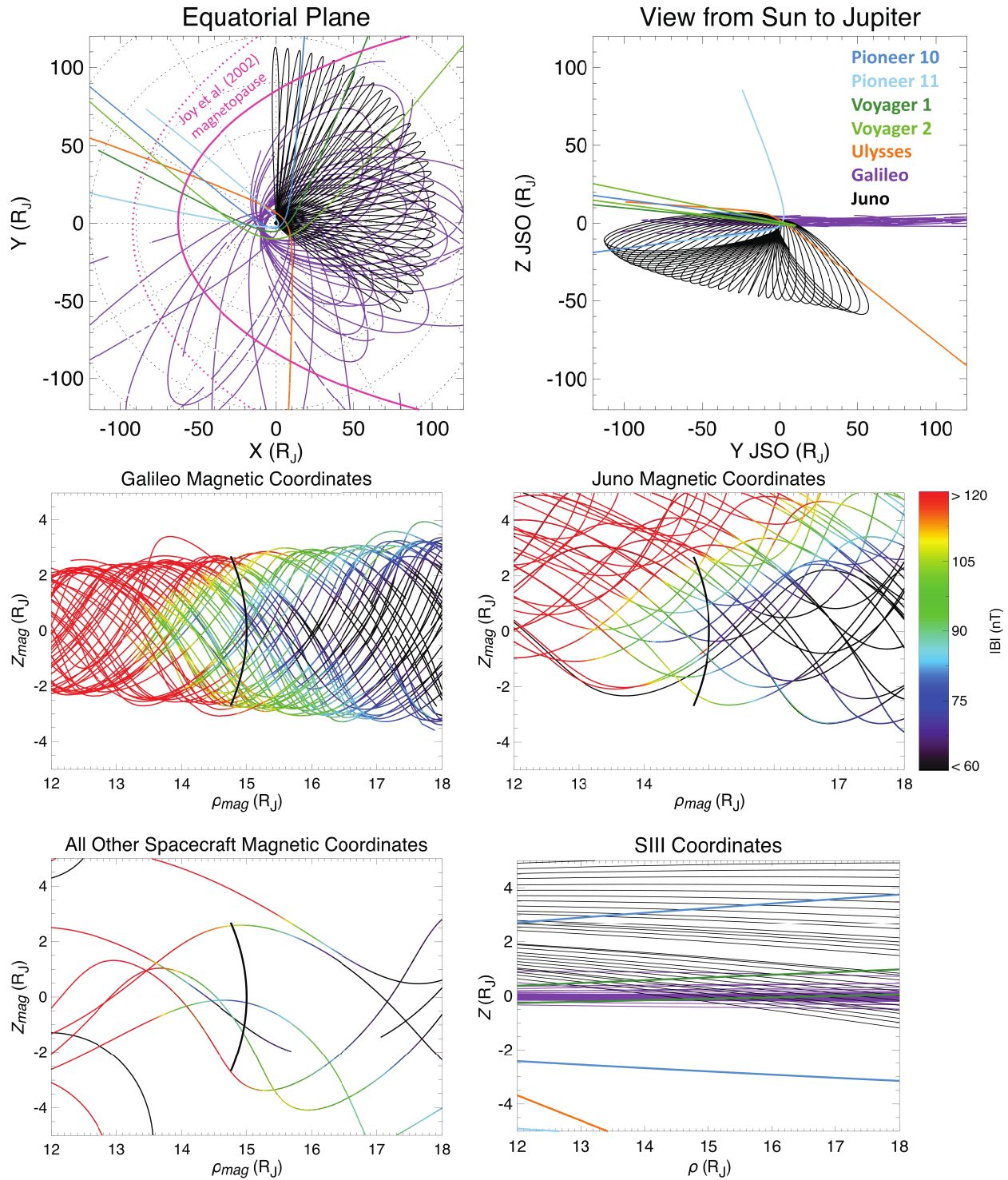
505 Palmaerts, B., Vogt, M. F., Krupp, N. , Grodent, D. and Bonfond, B. (2017). Dawn-Dusk
506 Asymmetries in Jupiter's Magnetosphere. In Dawn-Dusk Asymmetries in Planetary Plasma
507 Environments (eds S. Haaland, A. Runov and C. Forsyth). doi:10.1002/9781119216346.ch24
508
509 Phipps, P., & Bagenal, F. (2021). Centrifugal equator in Jupiter's plasma sheet. Journal of
510 Geophysical Research: Space Physics, 126, e2020JA028713., DOI:
511 <https://doi.org/10.1029/2020JA028713>
512
513 Russell, C. T., Z. J. Yu, K. K. Khurana, and M. G. Kivelson (2001), Magnetic field changes in
514 the inner magnetosphere of Jupiter, *Adv. Space Res.*, 28(6), 897-902.
515
516 Tao, C., R. Kataoka, H. Fukunishi, Y. Takahashi, and T. Yokoyama (2005), Magnetic field
517 variations in the Jovian magnetotail induced by solar wind dynamic pressure enhancements, *J.*
518 *Geophys. Res.*, 110, A11208, doi:10.1029/2004JA010959.
519
520 Tóth, G., Jia, X., Markidis, S., Peng, I. B., Chen, Y., Daldorff, L. K. S., Tenishev, V. M.,
521 Borovikov, D., Haiducek, J. D., Gombosi, T. I., et al. (2016), Extended magnetohydrodynamics
522 with embedded particle-in-cell simulation of Ganymede's magnetosphere, *J. Geophys. Res.*
523 *Space Physics*, 121, 1273– 1293, doi:10.1002/2015JA021997.
524
525 Vogt, M. F., E. J. Bunce, J. D. Nichols, J. T. Clarke, and W. S. Kurth (2017), Long-term
526 variability of Jupiter's magnetodisk and implications for the aurora, *Journal of Geophysical*
527 *Research: Space Physics*, 122, 12,090–12,110, doi:10.1002/2017JA024066.

528

529 Vogt, M. F., Gyalay, S., Kronberg, E. A., Bunce, E. J., Kurth, W. S., Zieger, B., & Tao, C.
530 (2019). Solar wind interaction with Jupiter's magnetosphere: A statistical study of Galileo in situ
531 data and modeled upstream solar wind conditions. *Journal of Geophysical Research: Space*
532 *Physics*, 124, 10170– 10199. <https://doi.org/10.1029/2019JA026950>

533

534 Zhou, H., Tóth, G., Jia, X., & Chen, Y. (2020). Reconnection-driven dynamics at Ganymede's
535 upstream magnetosphere: 3-D global Hall MHD and MHD-EPIC simulations. *Journal of*
536 *Geophysical Research: Space Physics*, 125, e2020JA028162.
537 <https://doi.org/10.1029/2020JA028162>

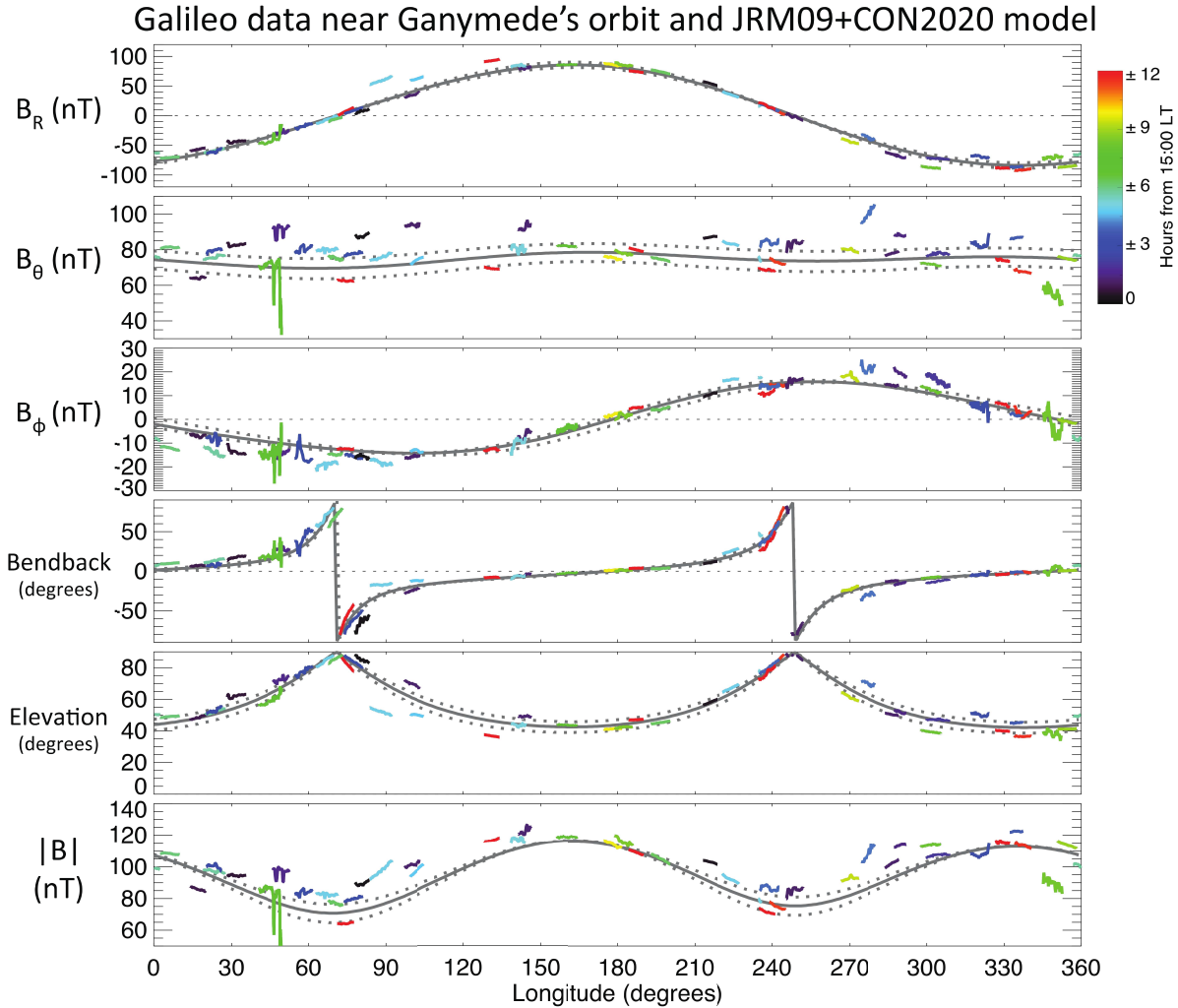


538

539 **Figure 1.** Trajectories of all spacecraft that have visited Jupiter's magnetosphere except Cassini
 540 and New Horizons. Top left: spacecraft trajectories projected onto the equatorial plane, with the
 541 Joy et al. (2002) magnetopause boundaries in pink. Top right: spacecraft trajectories as viewed

542 from the sun in JSO coordinates. Middle left: “wobble plot” showing Galileo’s orbital coverage
543 near Ganymede’s orbit, plotted in JRM09 magnetic cylindrical coordinates with color indicating
544 the measured magnetic field magnitude. The thick black line shows the possible range of
545 Ganymede’s location ($15 R_J$ radial distance and 0° jovigraphic latitude). Middle right: “wobble
546 plot” showing Juno’s orbital coverage near Ganymede’s orbit, plotted in JRM09 magnetic
547 cylindrical coordinates. Bottom left: “wobble plot” showing trajectories of Pioneers 10 and 11,
548 Voyagers 1 and 2, and Ulysses near Ganymede’s orbit, plotted in JRM09 magnetic cylindrical
549 coordinates. Bottom right: spacecraft trajectories in System III cylindrical coordinates near
550 Ganymede’s orbit.

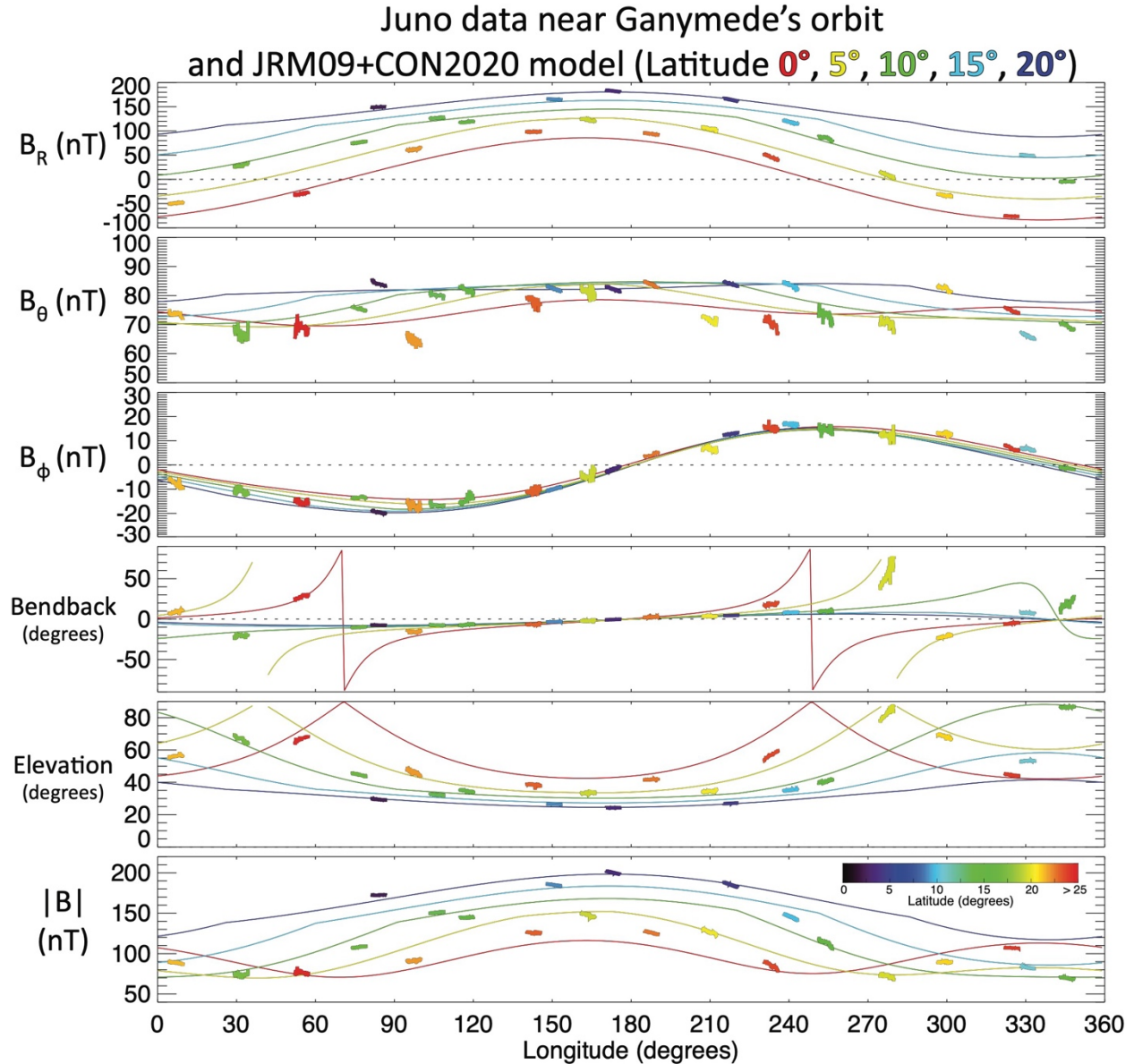
551



552

553 **Figure 2.** Dependence of the magnetic field near Ganymede’s orbit as a function of System III
 554 right-handed longitude, as measured by Galileo at radial distances 14.95-15.05 R_J , excluding the
 555 spacecraft’s six close flybys of Ganymede. From top: the radial (B_R), meridional (B_θ), and
 556 azimuthal (B_ϕ) components of the magnetic field in nT, the field bendback and elevation angles
 557 in degrees, and the field magnitude ($|B|$) in nT. Color indicates the number of hours of local time
 558 from 15:00. Gray solid lines show the field predicted by the average JRM09 + CON2020 model
 559 (Connerney et al., 2018, 2020) at Ganymede’s orbit while the dashed lines show the range of the
 560 expected field conditions based on model fits to individual Juno orbits (Connerney et al., 2020).

561

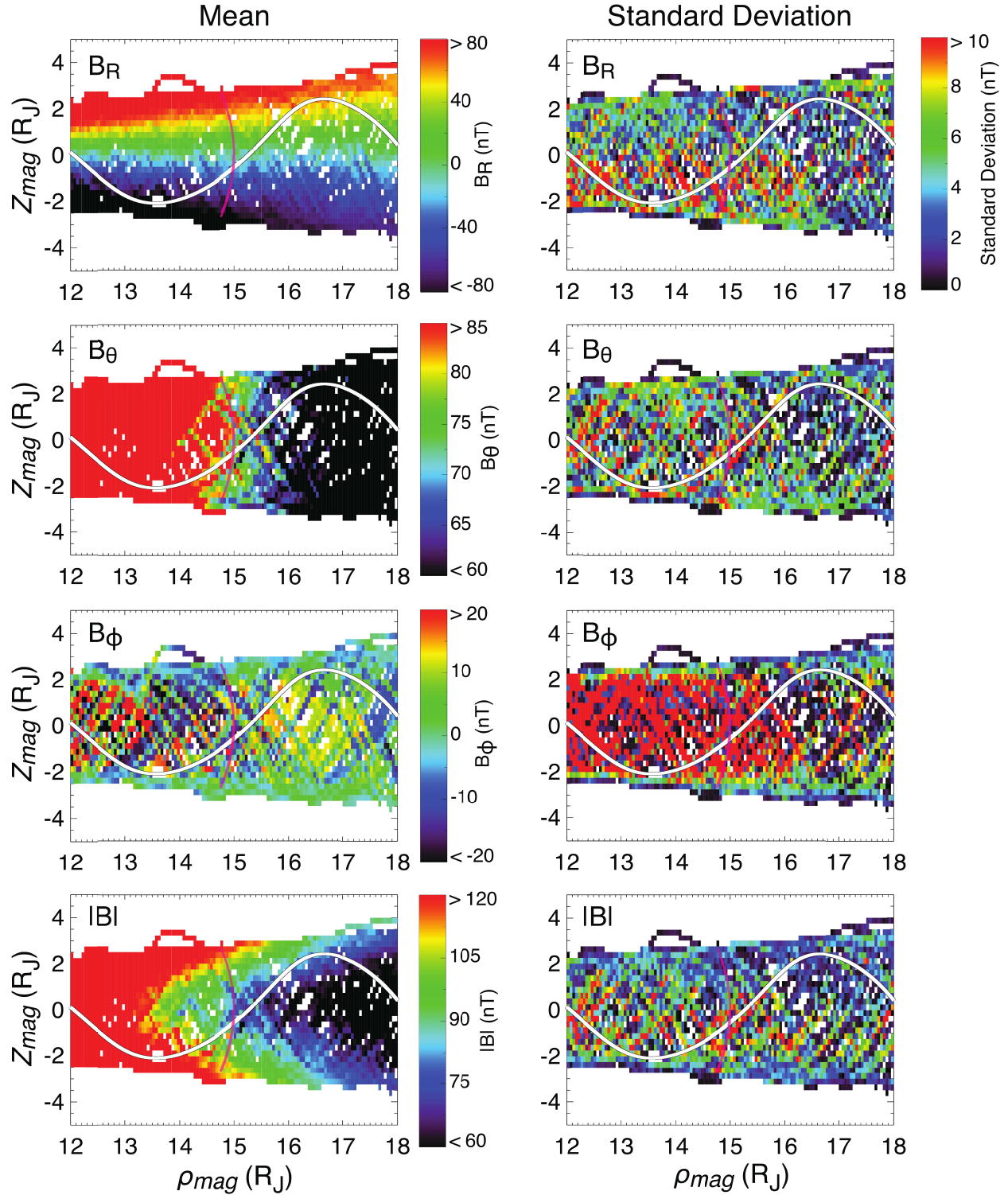


562

563 **Figure 3.** Dependence of the magnetic field near Ganymede's orbit as a function of System III
 564 right-handed longitude, from Juno's first 33 orbits at radial distances 14.95-15.05 R_J . From top:
 565 the radial (B_R), meridional (B_θ), and azimuthal (B_ϕ) components of the magnetic field in nT, the
 566 field bendback and elevation angles in degrees, and the field magnitude $|B|$ in nT. Data from each
 567 orbit are plotted with color indicating the average jovigraphic latitude of the spacecraft during
 568 the interval shown. The red solid line in each panel shows the quantity predicted by the JRM09 +
 569 CON2020 model (Connerney et al., 2018, 2020) at 15 R_J at the jovigraphic equator, while

570 yellow, green blue, and purple lines show the model predictions at 5°, 10°, 15°, and 20°
571 jovigraphic latitude, respectively.

572



573

574

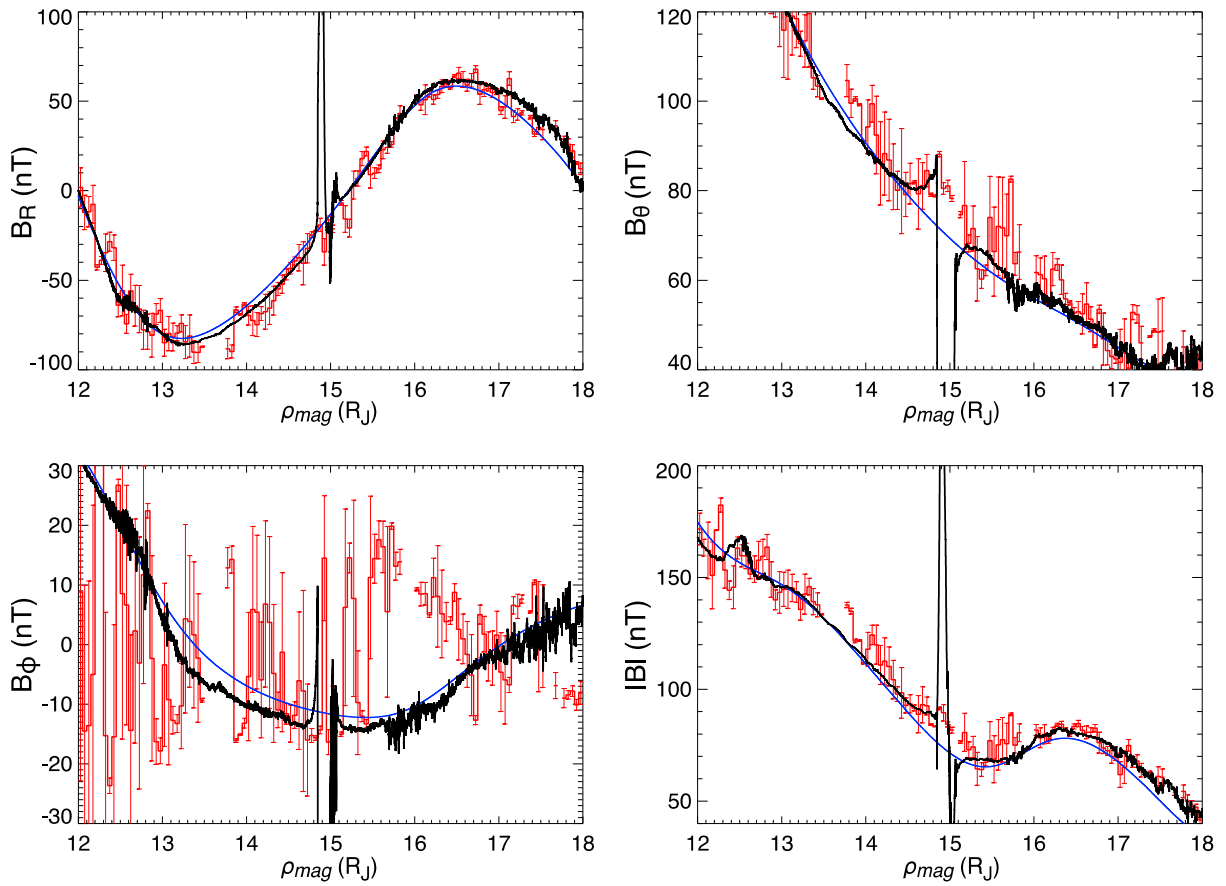
575

Figure 4. Magnetic field conditions measured by Galileo near Ganymede's orbit, organized in magnetic cylindrical coordinates. Boxes spanning $0.05 R_J$ in ρ_{mag} by $0.25 R_J$ in z_{mag} are drawn

576 with the color of each box indicating the mean measured magnetic field (left column) or standard
577 deviation of the measured magnetic field (right column) in each box. Thick white lines in each
578 panel show Juno's trajectory during orbit 34 and pink curves show the range of Ganymede's
579 possible positions.

580

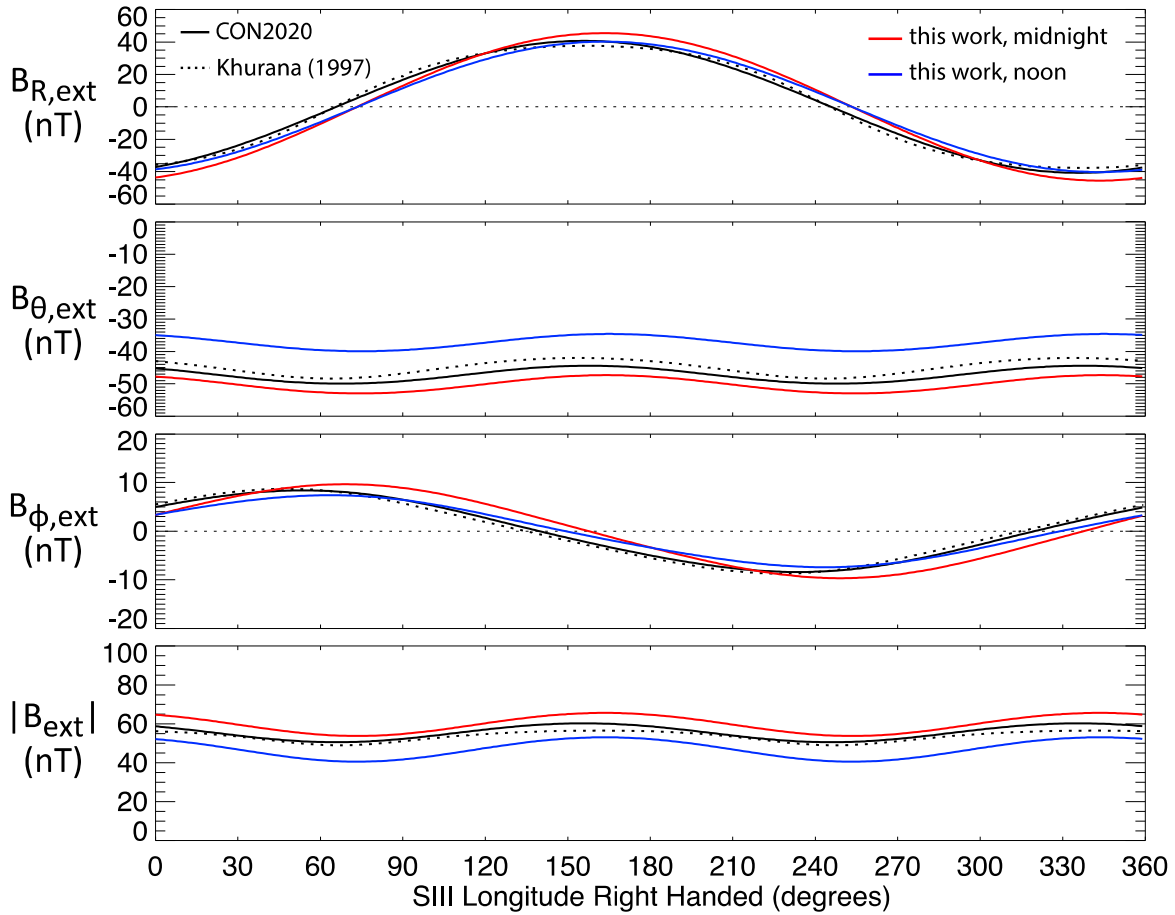
Juno Measured Field, Galileo Average, and JRM09+CON2020 model along Juno's orbit



581

582 **Figure 5.** Magnetic field components and magnitude measured by Juno during orbit 34 as a
 583 function of magnetic cylindrical distance ρ_{mag} . Also shown in red are the average magnetic field
 584 measured by Galileo, with error bars indicating the standard deviation, along Juno's trajectory in
 585 magnetic coordinates, calculated in bins of $0.05 R_J$ in ρ_{mag} and $0.25 R_J$ in z_{mag} . Blue lines show
 586 the JRM09+CON2020 model field.

587



588

589 **Figure A1.** Modeled external field at radial distance $15 R_J$ in the jovigraphic equator from the

590 CON2020 model (black solid lines), Khurana (1997) model (black dashed lines), and the

591 functional fits described in equations A1-A3 evaluated at noon (blue) and midnight (red) local

592 times, plotted as a function of longitude. From top: the radial (B_R), meridional (B_θ), and

593 azimuthal (B_ϕ) components of the magnetic field, and the field magnitude ($|B|$), all in nT.

594

595

596
597

Table 1. Measured^a and modeled magnetic field values and field angles near Ganymede’s orbit

	Minimum (excepting orbit C9 ^b)	Maximum (all orbits)	Minimum (Orbit C9 only ^a)	JRM09 + CON2020 model minimum ^b	JRM09 + CON2020 model maximum ^b	JRM09 + CON2020 model average ^c	Average variability due to change in CON2020 current constants ^d
B_R (nT)	-92.78	95.15		-83.80	85.61	53.9	~6 nT
B_θ (nT)	48.50	105.50	32.06	69.54	78.55	74.36	~11 nT
B_ϕ (nT)	-21.91	25.12	-27.10	-14.28	15.83	9.47	~2 nT
$ B $ (nT)	63.76	126.59	37.24	70.76	116.2	94.95	~5 nT
Bendback angle ^e (degrees)	-82.43	82.06		-88.43	86.62	17.39	~4°
Elevation angle ^e (degrees)	33.75	88.61		42.15	89.72	56.30	~6°

598 ^a Galileo measurements at radial distances 14.95-15.05 R_J excepting the six close flybys of
599 Ganymede, at near-jovigraphic latitudes (-1.57° to 3.27°)

600 ^b The magnetic field measured during orbit C9, which occurred near 50° longitude, was
601 anomalously small due to a likely current sheet crossing, which affects the minimum observed
602 B_θ , B_ϕ , and $|B|$.

603 ^c Model values were calculated at 15.0 R_J , 0° latitude, and from 0° to 360° longitude in 1°
604 increments, using the average CON2020 current constant fit values.

605 ^d Averages and variability are calculated using $|B_R|$, $|B_\phi|$, and the magnitude of the field
606 bendback angle.

607 ^e Field angles are not calculated when $|B_R| < 3$ nT.

608

609 **Table 2.** JRM09 + CON2020 model prediction at Ganymede's orbit^a during the Juno flyby

	50° longitude, average	50° longitude, expected temporal variability	70° longitude, average	70° longitude, expected temporal variability
B_R (nT)	-28.3	-29.6 – -27.1	-1.1	-0.7 – -1.4
B_θ (nT)	69.9	64.1 – 75.3	69.6	63.7 – 75.5 ⁹¹⁵ 71.6
B_ϕ (nT)	-10.2	-8.7 – -11.4	-11.5	-11.7 – -13.4
$ B $ (nT)	76.1	71.2 – 80.8	72.1	64.8 – 76.3 ⁸¹⁷ 81.8
Bendback angle	19.9°	16.3° – 22.8°	37.5°	86.6° – 84.1°
Elevation angle (degrees)	67.9°	65.2° – 70.2°	77.9°	89.4° – 88.9° 621 622 623

624 ^aModel field computed at 15 R_J radial distance and 0° jovigraphic latitude

625

626 **Table A1.** Root mean square error between the field model and Galileo measurements at 14.95
 627 $R_J < R < 15.05 R_J$ (excepting orbit C9)

Model	B_R RMS Error (nT)	B_θ RMS Error (nT)	B_ϕ RMS Error (nT)	$ B $ RMS Error (nT)
JRM09 (full model) + CON2020	7.12	9.24	3.42	8.93
JRM09 (full model) + Khurana (1997) with V2 parameters ^a	7.65	8.74	3.53	7.91
JRM09 dipole + this work	8.50	6.46	3.01	7.76
JRM09 full model + this work	8.03	6.01	3.17	7.11

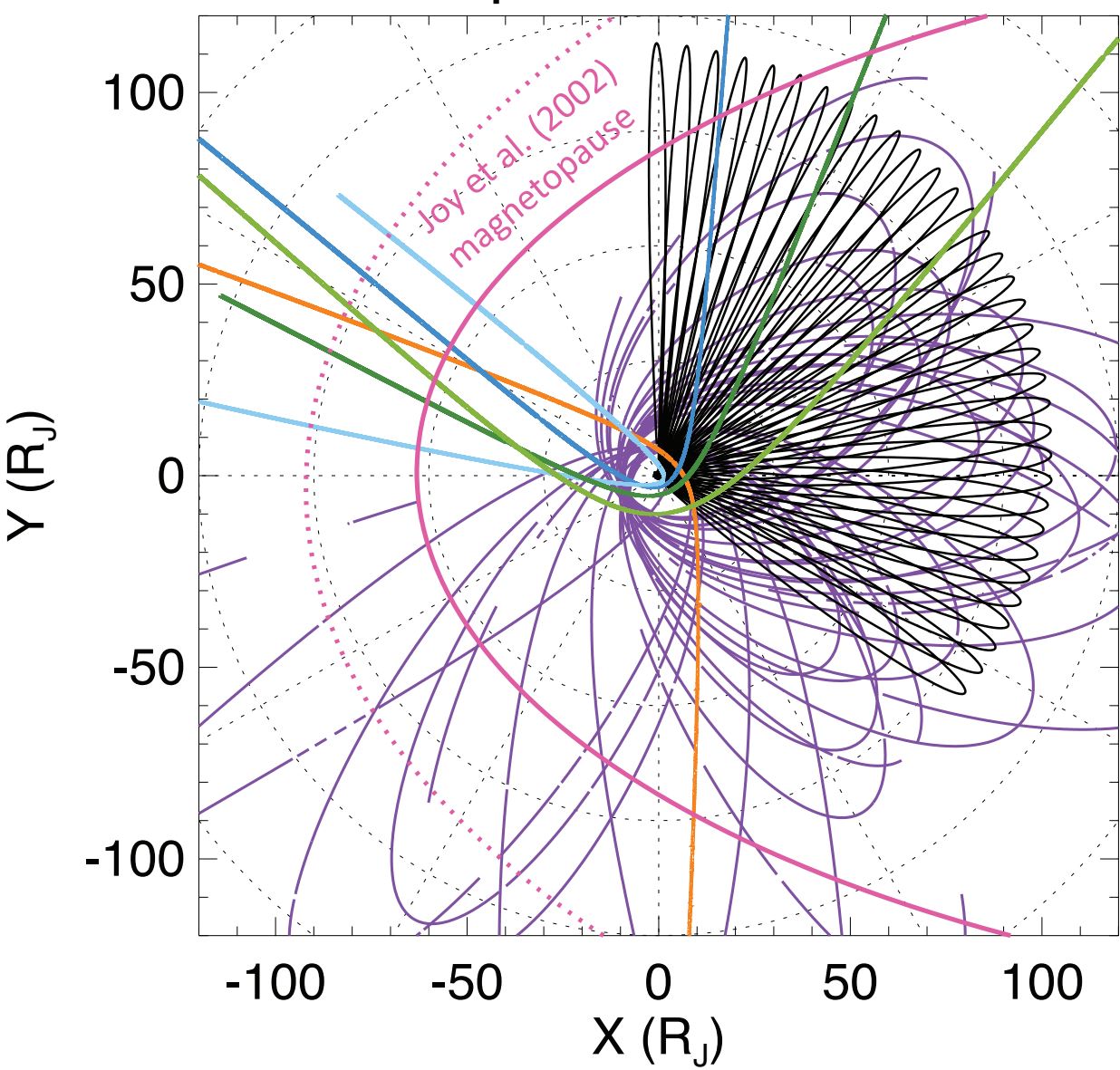
628 ^a Khurana (1997) fit model parameters separately to Voyager 1, Voyager 2, and Pioneer 10 data
 629 and also provided a set of “common model” fit parameters obtained using data from all three
 630 spacecraft. For B_θ , B_ϕ , and $|B|$, the smallest RMS errors between Galileo data and the
 631 JRM09+K97 are obtained when using the V2 parameters and the largest RMS errors are obtained
 632 using the V1 parameters. For B_R , the “common model” parameters produce the smallest RMS

633 error (6.63 nT – though the overall $|B|$ RMS error is 10.29 nT) while the V2 parameters produce
634 the largest RMS error.

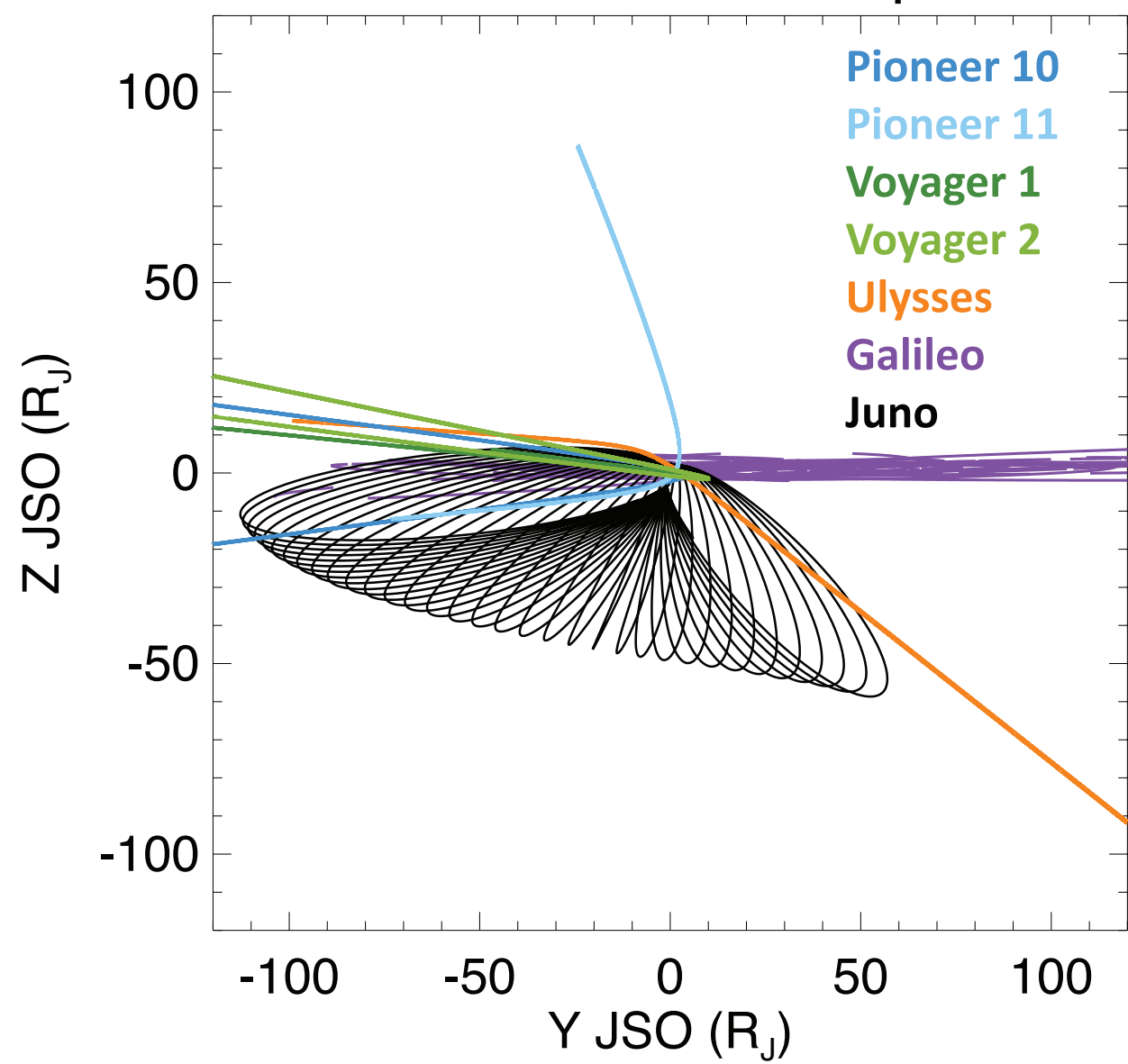
635

Figure 1.

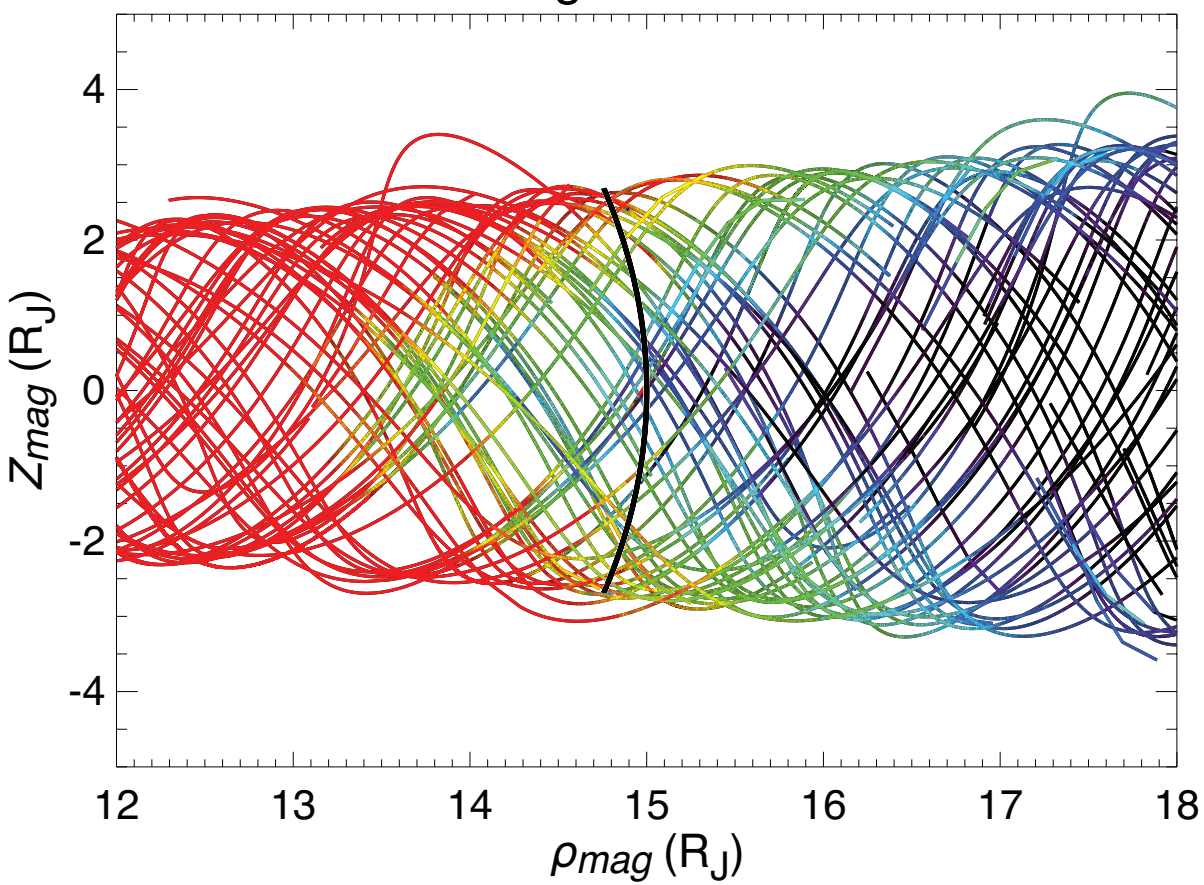
Equatorial Plane



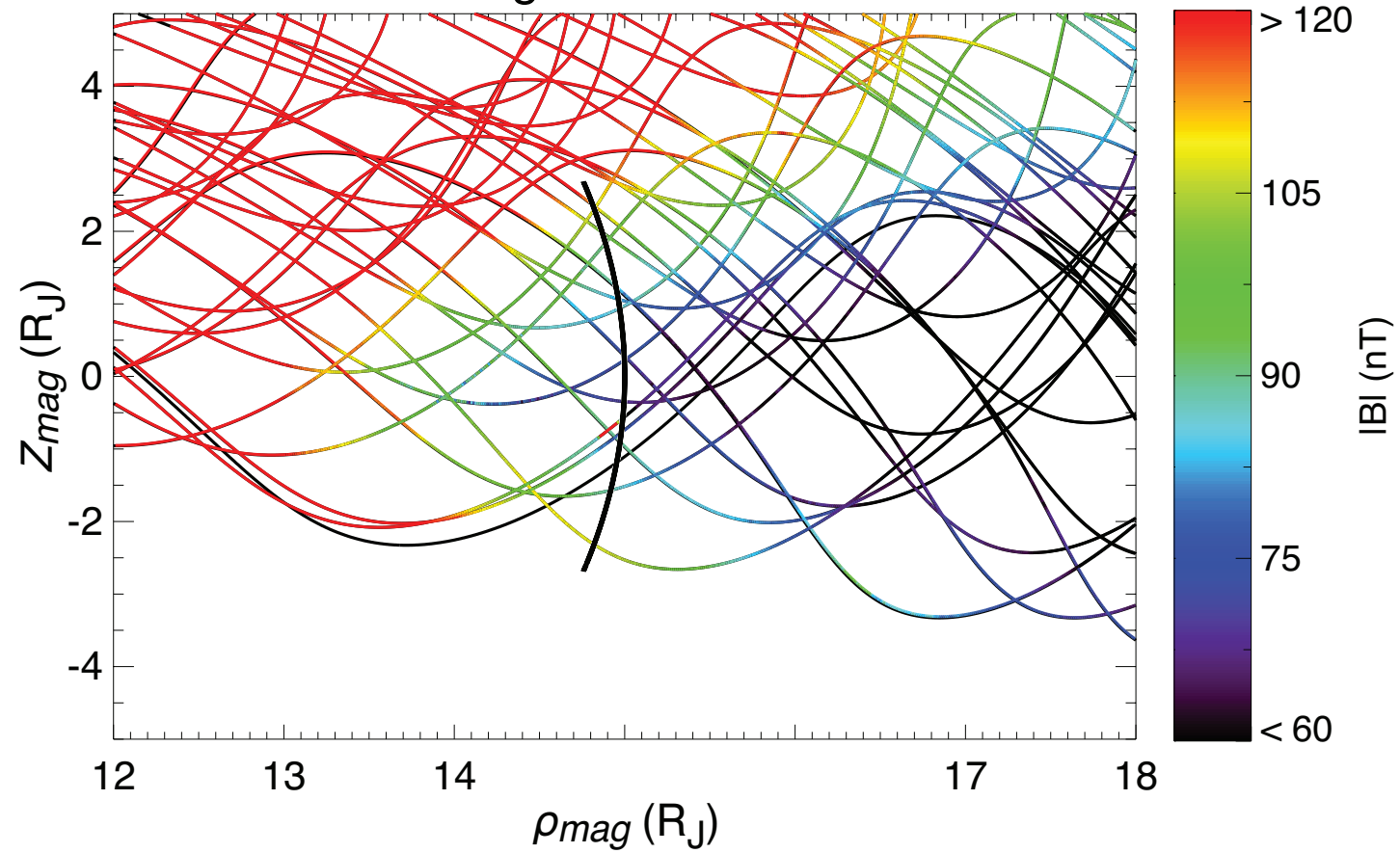
View from Sun to Jupiter



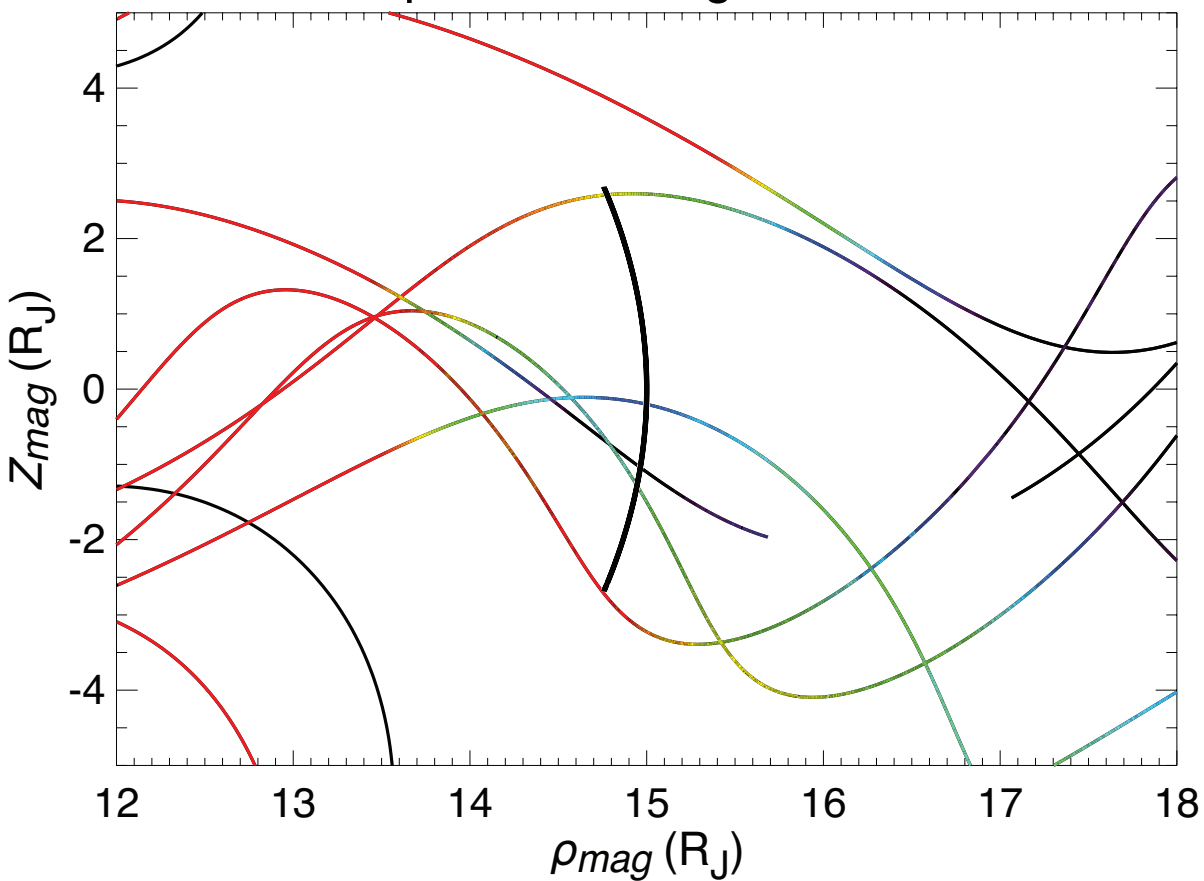
Galileo Magnetic Coordinates



Juno Magnetic Coordinates



All Other Spacecraft Magnetic Coordinates



SIII Coordinates

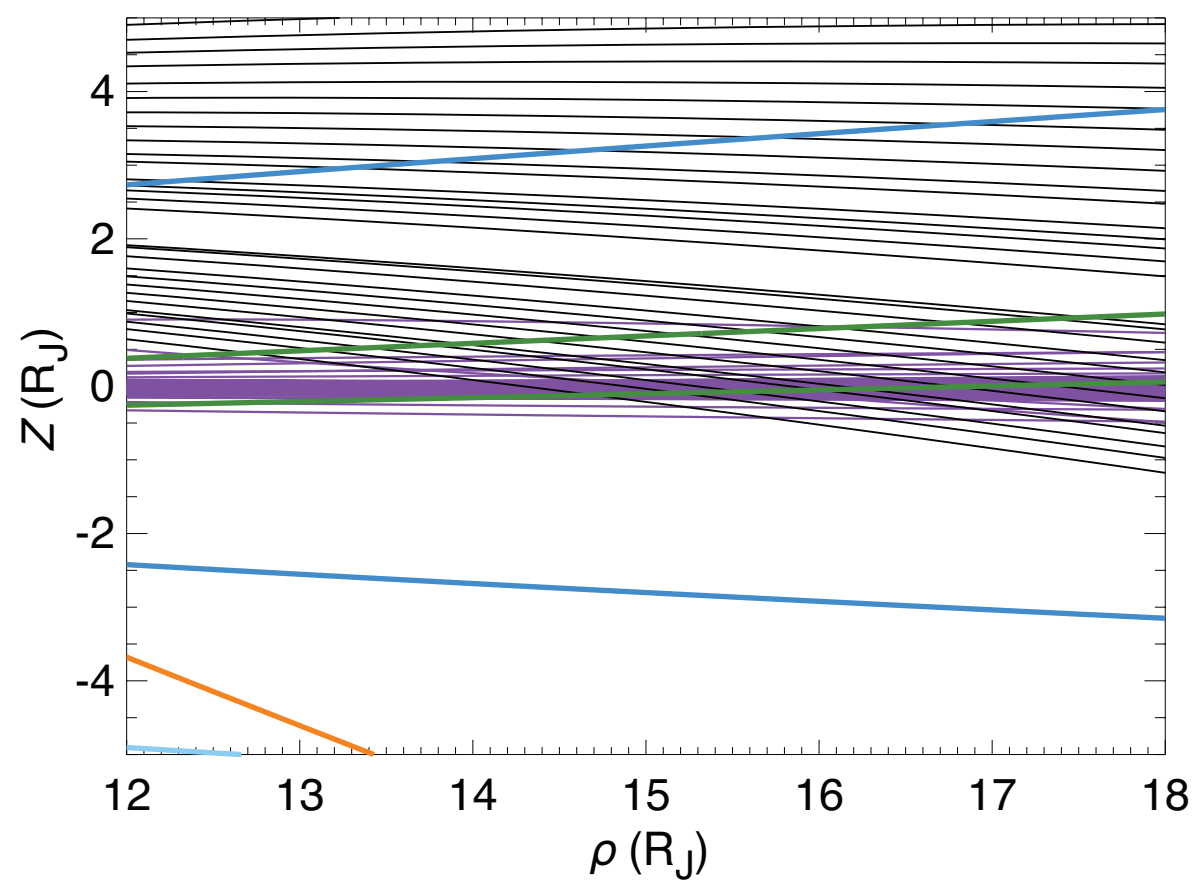


Figure 2.

Galileo data near Ganymede's orbit and JRM09+CON2020 model

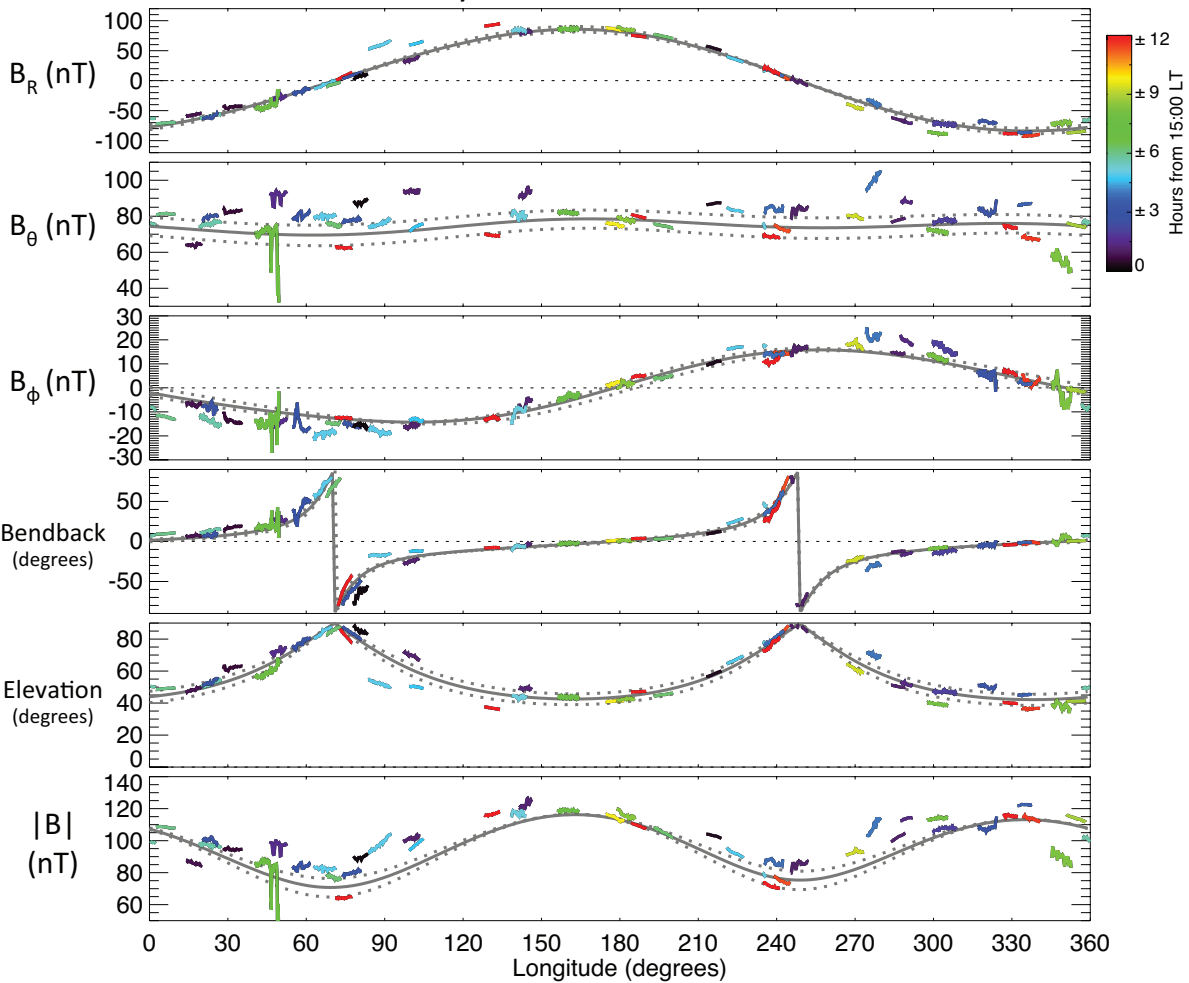


Figure 3.

Juno data near Ganymede's orbit and JRM09+CON2020 model (Latitude 0° , 5° , 10° , 15° , 20°)

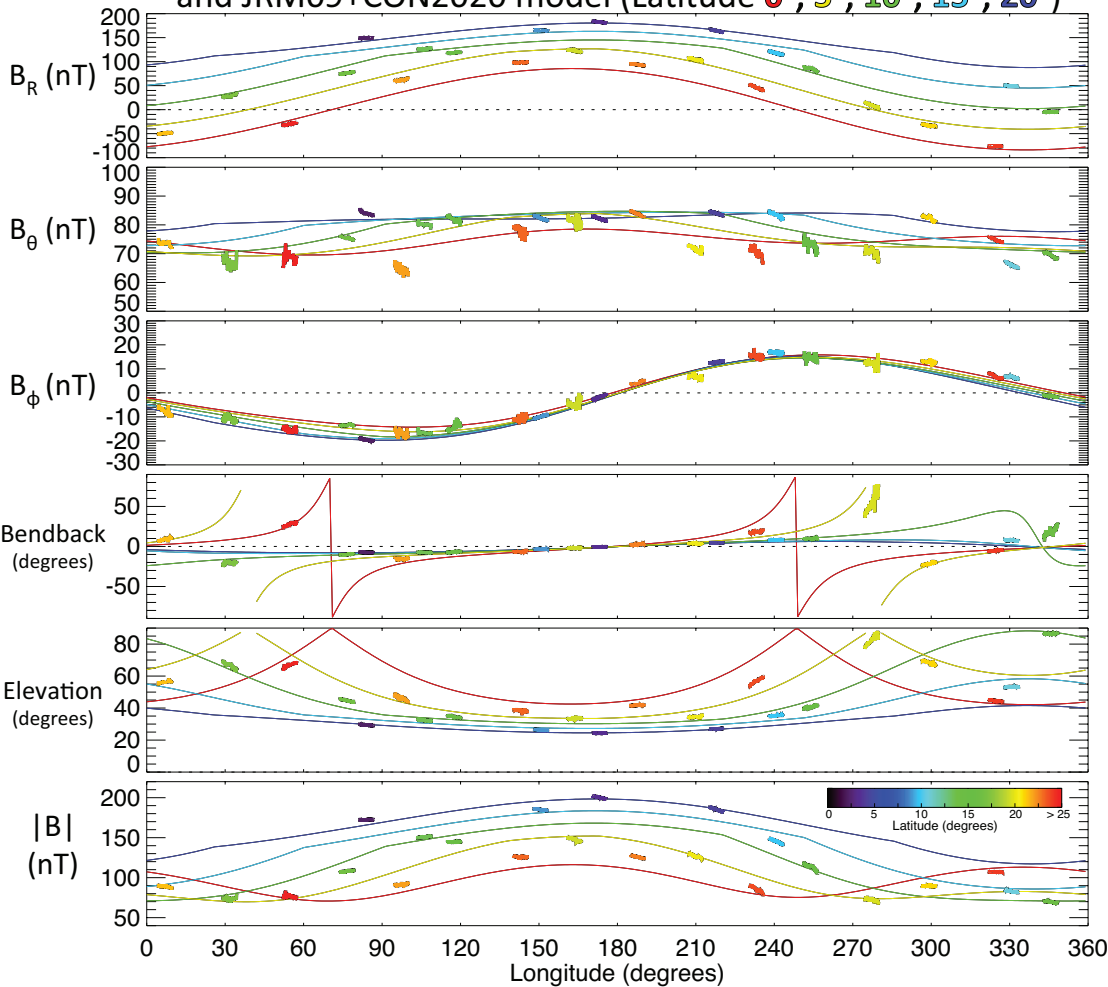


Figure 4.

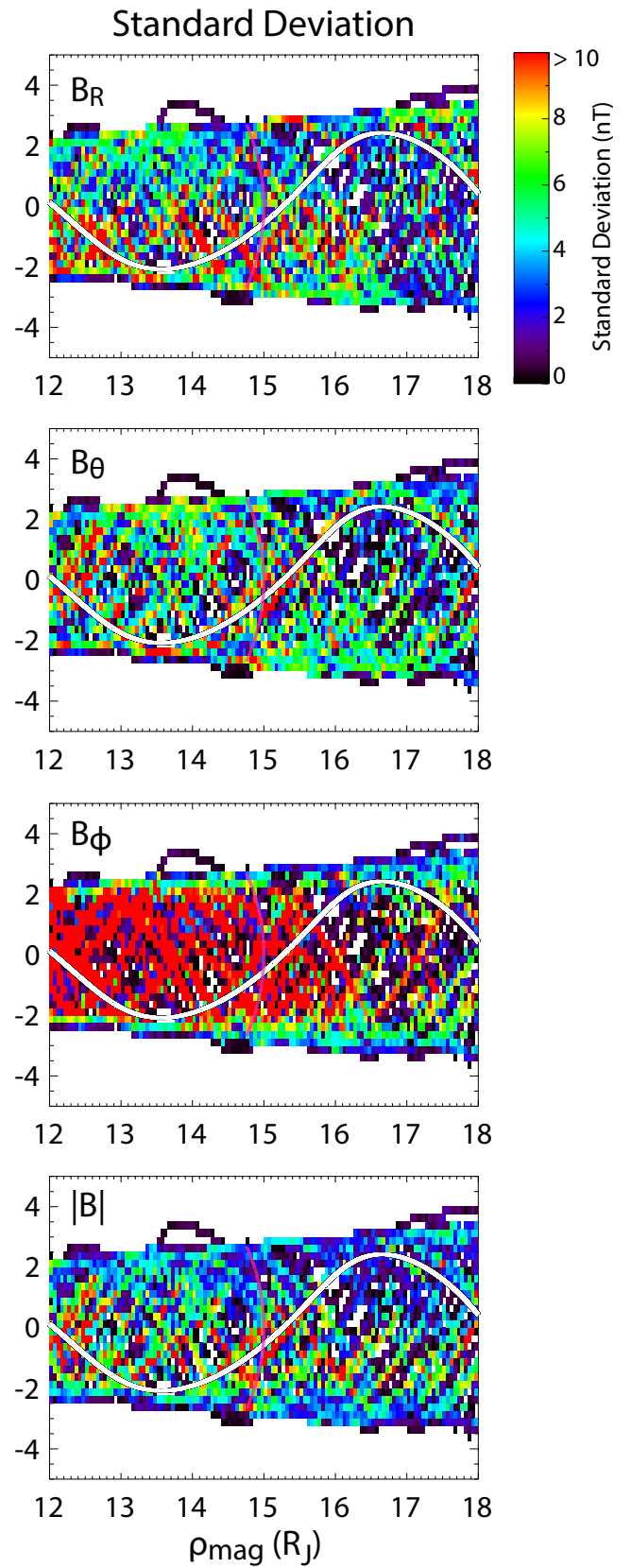
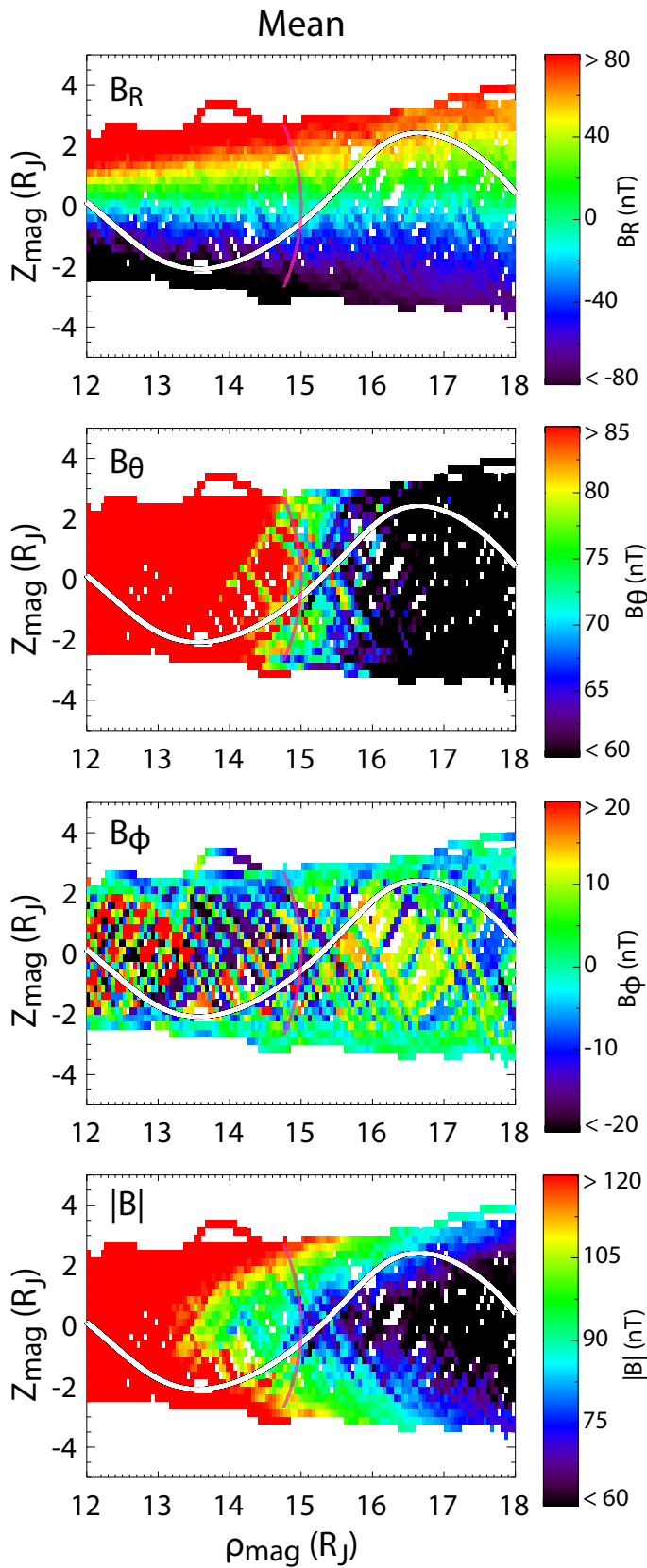


Figure 5.

Juno Measured Field, Galileo Average, and JRM09+CON2020 model along Juno's orbit

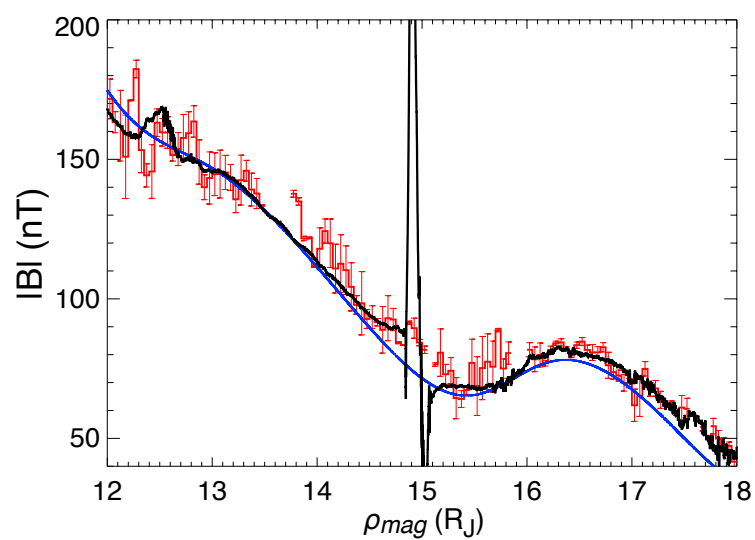
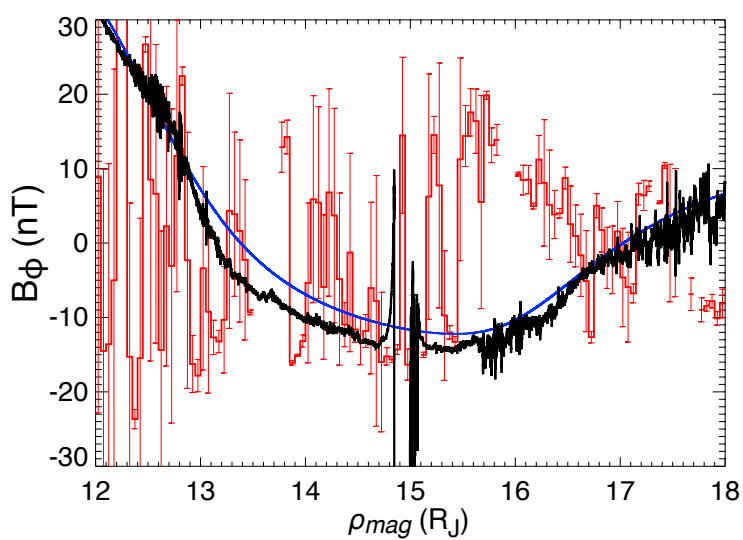
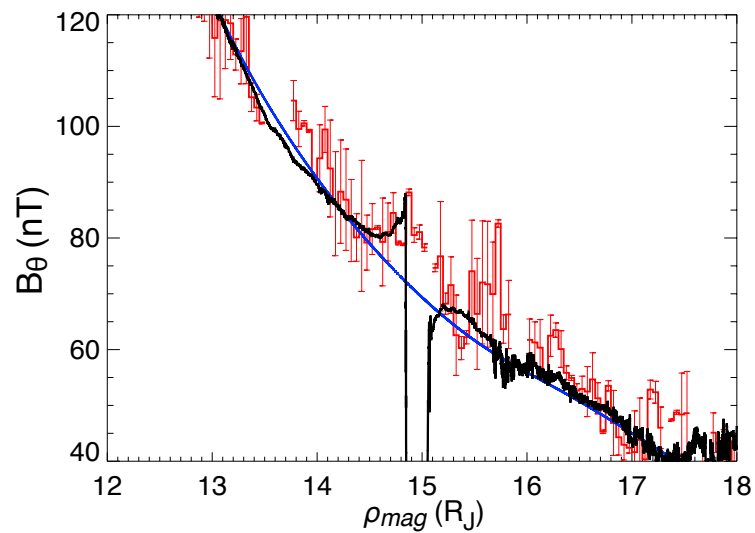
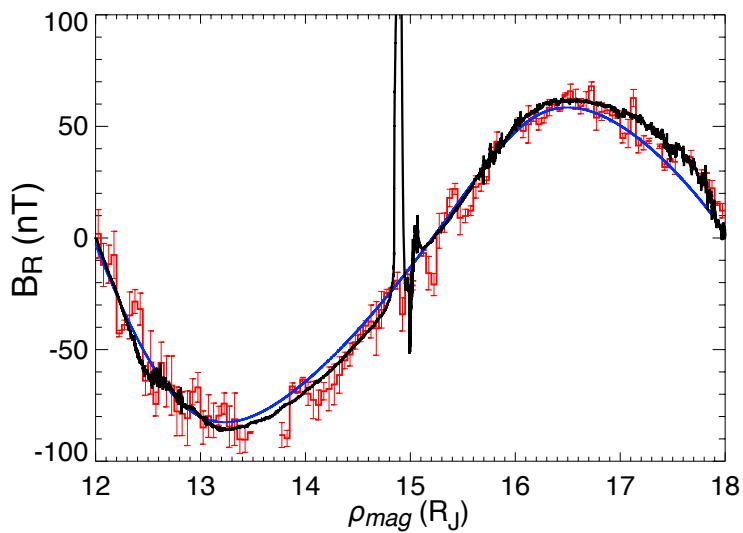


Figure A1.

